World Journal of Gastroenterology

Submit a Manuscript: https://www.f6publishing.com

World J Gastroenterol 2024 August 7; 30(29): 3511-3533

DOI: 10.3748/wjg.v30.i29.3511

ISSN 1007-9327 (print) ISSN 2219-2840 (online)

ORIGINAL ARTICLE

Basic Study

Calculus bovis inhibits M2 tumor-associated macrophage polarization *via* Wnt/β-catenin pathway modulation to suppress liver cancer

Zhen Huang, Fan-Ying Meng, Lin-Zhu Lu, Qian-Qian Guo, Chang-Jun Lv, Nian-Hua Tan, Zhe Deng, Jun-Yi Chen, Zi-Shu Zhang, Bo Zou, Hong-Ping Long, Qing Zhou, Sha Tian, Si Mei, Xue-Fei Tian

Specialty type: Gastroenterology and hepatology

Provenance and peer review: Unsolicited article; Externally peer reviewed.

Peer-review model: Single blind

Peer-review report's classification

Scientific Quality: Grade B, Grade B, Grade B, Grade C, Grade C, Grade C

Novelty: Grade A, Grade B, Grade B, Grade B, Grade C, Grade C

Creativity or Innovation: Grade A, Grade B, Grade B, Grade B, Grade B, Grade C

Scientific Significance: Grade A, Grade B, Grade B, Grade B, Grade B, Grade D

P-Reviewer: Buldak L; Ricci AD; Rizzo A; Shelat VG

Received: April 9, 2024

Revised: June 5, 2024

Accepted: July 5, 2024

Published online: August 7, 2024

Processing time: 110 Days and 21.6 Hours

Zhen Huang, Lin-Zhu Lu, Qian-Qian Guo, Chang-Jun Lv, Nian-Hua Tan, Zhe Deng, Jun-Yi Chen, Sha Tian, Xue-Fei Tian, College of Integrated Chinese and Western Medicine, Hunan University of Chinese Medicine, Changsha 410208, Hunan Province, China

Zhen Huang, Lin-Zhu Lu, Qian-Qian Guo, Chang-Jun Lv, Nian-Hua Tan, Jun-Yi Chen, Si Mei, Xue-Fei Tian, Hunan Key Laboratory of Translational Research in Formulas and Zheng of Traditional Chinese Medicine, Hunan University of Chinese Medicine, Changsha 410208, Hunan Province, China

Zhen Huang, Lin-Zhu Lu, Qian-Qian Guo, Chang-Jun Lv, Nian-Hua Tan, Jun-Yi Chen, Si Mei, Xue-Fei Tian, Key Laboratory of Traditional Chinese Medicine for Mechanism of Tumor Prevention and Treatment, Hunan University of Chinese Medicine, Changsha 410208, Hunan Province, China

Fan-Ying Meng, Zi-Shu Zhang, Bo Zou, The First Clinical College of Traditional Chinese Medicine, Hunan University of Traditional Chinese Medicine, Changsha 410007, Hunan Province, China

Nian-Hua Tan, Department of Hepatology, Hunan University of Chinese Medicine, Changsha 410007, Hunan Province, China

Hong-Ping Long, Qing Zhou, The First Hospital of Hunan University of Chinese Medicine, Hunan University of Chinese Medicine, Changsha 410007, Hunan Province, China

Si Mei, Faculty of Medicine, Hunan University of Chinese Medicine, Changsha 410208, Hunan Province, China

Co-first authors: Zhen Huang and Fan-Ying Meng.

Co-corresponding authors: Si Mei and Xue-Fei Tian.

Corresponding author: Xue-Fei Tian, College of Integrated Chinese and Western Medicine, Hunan University of Chinese Medicine, No. 300 Xueshi Road, Changsha 410208, Hunan Province, China. 003640@hnucm.edu.cn

Abstract

BACKGROUND

Calculus bovis (CB), used in traditional Chinese medicine, exhibits anti-tumor effects in various cancer models. It also constitutes an integral component of a compound formulation known as Pien Tze Huang, which is indicated for the treatment of liver cancer. However, its impact on the liver cancer tumor microenvironment, particularly on tumor-associated macrophages (TAMs), is not well understood.

AIM

To elucidate the anti-liver cancer effect of CB by inhibiting M2-TAM polarization *via* Wnt/β-catenin pathway modulation.

METHODS

This study identified the active components of CB using UPLC-Q-TOF-MS, evaluated its anti-neoplastic effects in a nude mouse model, and elucidated the underlying mechanisms *via* network pharmacology, transcriptomics, and molecular docking. *In vitro* assays were used to investigate the effects of CB-containing serum on HepG2 cells and M2-TAMs, and Wnt pathway modulation was validated by real-time reverse transcriptase-polymerase chain reaction and Western blot analysis.

RESULTS

This study identified 22 active components in CB, 11 of which were detected in the bloodstream. Preclinical investigations have demonstrated the ability of CB to effectively inhibit liver tumor growth. An integrated approach employing network pharmacology, transcriptomics, and molecular docking implicated the Wnt signaling pathway as a target of the antineoplastic activity of CB by suppressing M2-TAM polarization. *In vitro* and *in vivo* experiments further confirmed that CB significantly hinders M2-TAM polarization and suppresses Wnt/β-catenin pathway activation. The inhibitory effect of CB on M2-TAMs was reversed when treated with the Wnt agonist SKL2001, confirming its pathway specificity.

CONCLUSION

This study demonstrated that CB mediates inhibition of M2-TAM polarization through the Wnt/β-catenin pathway, contributing to the suppression of liver cancer growth.

Key Words: *Calculus bovis*; M2 tumor-associated macrophage polarization; Liver cancer; Wnt/β-catenin pathway; Tumor microenvironment

©The Author(s) 2024. Published by Baishideng Publishing Group Inc. All rights reserved.

Core Tip: *Calculus bovis* (CB), a valuable herb in traditional Chinese medicine, has shown definite anti-liver cancer effects *in vivo*. By analyzing the composition of CB and using network pharmacology for target prediction, we found that CB exhibits anti-liver cancer effects by affecting immune-related pathways in the tumor microenvironment. Through transcriptome sequencing, we further showed that regulation of the M2-type polarization of tumor-associated macrophages (TAMs) is responsible for the effects of CB. *In vitro* studies showed that modulating the Wnt/β-catenin pathway is a crucial mechanism by which CB regulates M2 polarization of TAMs. This study provides evidence for the development of anti-liver cancer drugs.

Citation: Huang Z, Meng FY, Lu LZ, Guo QQ, Lv CJ, Tan NH, Deng Z, Chen JY, Zhang ZS, Zou B, Long HP, Zhou Q, Tian S, Mei S, Tian XF. *Calculus bovis* inhibits M2 tumor-associated macrophage polarization *via* Wnt/β-catenin pathway modulation to suppress liver cancer. *World J Gastroenterol* 2024; 30(29): 3511-3533
URL: https://www.wjgnet.com/1007-9327/full/v30/i29/3511.htm
DOI: https://dx.doi.org/10.3748/wjg.v30.i29.3511

INTRODUCTION

Liver cancer is a global health concern that ranks sixth in prevalence and fourth in cancer-related mortality worldwide [1]. Liver cancer is highly malignant, progresses rapidly, and has a poor prognosis. The 5-year survival rate of patients with liver cancer is only 3%, severely affecting their quality of life[2]. The primary treatment options for liver cancer include surgical interventions such as liver resection or transplantation, interventional therapies, local ablation treatments, and targeted immunotherapies[3-6]. However, the application of these treatments has limitations, and the survival rate of some patients remains low even after treatment[7-10]. Therefore, there is an urgent need for novel and more effective strategies for the treatment of liver cancer[11,12]. Traditional Chinese medicine (TCM) is characterized by a

multicomponent and multi-target approach[13,14]. Studies have shown that TCM can inhibit liver cancer by regulating the tumor microenvironment (TME)[15], offering a new perspective on liver cancer treatment. Within the multifaceted TME, macrophages play a crucial role in liver cancer progression[16]. Tumor-associated macrophages (TAMs) derived from circulating monocytes can adopt the M1 or M2 phenotype in response to various TME cytokines and growth factors [17]. While M1-type TAMs exhibit anti-tumor properties driven by cytokines such as IFN-γ and TNF-α[18], M2 TAMs (M2-TAMs) support tumor growth and metastasis through pathways such as NF-κB, IL-6/STAT3, and Wnt/β-catenin[19-21]. These pathways also facilitate TAM-mediated tumor proliferation, invasion, and angiogenesis[22,23]. Therefore, reversing TAM polarization and targeting these pathways are promising therapeutic approaches for liver cancer.

TCM values *Calculus bovis* (CB) for its anti-tumor potential in various models[24]. Combinations of CB with Moschus have been shown to induce apoptosis in liver cancer cells such as SMMC-7721 and HepG2[25,26]. Prior research has documented the mechanisms of CB against liver cancer[27] and its ability to enhance macrophage phagocytosis while suppressing pro-inflammatory cytokine secretion and alleviating liver inflammation and injury[28]. However, the full extent of the influence of CB on the liver cancer TME, particularly on TAMs, remains elusive.

This investigation revealed that the antineoplastic effects of CB may involve the inhibition of M2-polarized TAM differentiation through the modulation of key molecular pathways. Our comprehensive *in vitro* and *in vivo* analyses aimed to elucidate the mechanisms underlying the anti-liver cancer activity of CB, including its active constituents, cellular targets, and signaling pathways. The findings demonstrated the regulatory role of CB in macrophage phenotypic plasticity and interaction with the Wnt/β-catenin pathway within the TME. This study lays a foundation for developing CB-derived antineoplastic therapeutic strategies that inhibit M2-TAM polarization by targeting the Wnt/β-catenin pathway to suppress liver cancer.

MATERIALS AND METHODS

Chemicals and reagents

CB (20160526-2) was obtained from Hunan Sanxiang Herbal Pieces Co., Ltd. (Hunan, China). Sorafenib was obtained from GLPbio, Inc. (Montclair, United States). HepG2 cells, fetal bovine serum (FBS), and Dulbecco's modified Eagle's medium (DMEM) were acquired from Meisen Cell Technology Co., Ltd. (Zhejiang, China). HepG2 cells were authenticated using short tandem repeats. THP-1 cells were provided by the State Key Laboratory of Macau University. The TRIzol Kit (15596026) was procured from Thermo Fisher Scientific (Massachusetts, United States). Phorbol 12-myristate 13-acetate (PMA) and the cytokines for cell induction, including IL-4 and IL-13, were procured from Sigma (Darmstadt, United States). The Cell Counting Kit-8 (CCK-8) Kit was procured from Biosharp (Anhui, China). The Annexin V-FITC/PI Apoptosis Kit was purchased from APExBIO (Houston, TX, United States). Type I collagenase was purchased from BioFroxx (Santiago, Germany). A Protein Assay Kit was purchased from CWBIO (Jiangsu, China). NovoStart®SYBR qPCR SuperMix Plus, and NovoScript®Plus All-in-one 1st Strand cDNA Synthesis SuperMix were procured from Novoprotein Inc. (Jiangsu, China). The primary antibodies against Wnt5B (#55184-1-AP), β-catenin (#66379-1-Ig), Axin2 (#20540-1-AP), and GADPH (#66009-1-Ig), as well as HRP-conjugated affinipure goat anti-rabbit IgG (#SA00001-2) and multi-rab HRP-goat anti-mouse recombinant secondary antibody (#RGAMΦ01), were acquired from Proteintech (Wuhan, China).

In vivo and in vitro analysis of CB components

Sample preparation: To prepare a CB extract, 2.0 g of CB was mixed with 30 mL of 100% methanol, followed by ultrasonication for 30 min at 250 W and 40 kHz. After ultrasonication, the mixture was allowed to settle. Next, 2 mL of the mixture was centrifuged at 8000 *g* at 25 °C for 5 min. The supernatant was then filtered using a 0.22 μm microporous membrane, and 1 mL of this filtrate was reserved in an injection vial for subsequent analysis.

For serum sample preparation, 2 mL of CB-enriched serum and 2 mL of blank serum (BS) were taken separately, and each was mixed with 6 mL of 100% methanol. The mixtures were chilled in an ice bath, then centrifuged at 12000 g at 25 °C for 5 min. The supernatant was then dried using a centrifugal evaporator. The dried samples were re-dissolved in 100 μL methanol and again centrifuged under the same conditions to ensure clarity. Finally, the purified supernatants were filtered with a 0.22 μm microporous membrane for further examination.

Chromatography and mass spectrometry: Chromatographic analysis was conducted using an Agilent ZORBAX Eclipse Plus C18 column, applying a gradient elution method with mobile phases of acetonitrile and either 1 mL/L formic acid in water in the positive ion mode or 5 mmol/L ammonium acetate in water in the negative ion mode. The sample injection volume was 2 μL. Subsequently, mass spectrometry (MS) was performed with both positive and negative ESI settings, utilizing a multi-reaction monitoring scanning mode and calibrated with the ESI-L Low Concentration Tuning Mix. The MS spanned m/z 100 to 1500 with a resolution of 30000, employing nitrogen as the nebulizing gas, and a drying temperature of 325 °C, capillary voltage of 4.0 kV, fragmentation voltage of 110 V, and sheath gas temperature of 350 °C were maintained.

Animal experiments

Subcutaneous transplantation tumor experiment: Male 6-wk-old *BALB/c* nude mice and Sprague-Dawley rats, supplied by Hunan Slake Jinda Laboratory Animal Company Limited (Changsha, China), were housed under specific pathogen-free conditions. All animals were maintained in an environment with a controlled 12-hour dark/light cycle at 21 ± 2 °C and 50% ± 10% relative humidity.

Nude mouse xenograft tumors were induced *via* subcutaneous injection of 5 × 10^6 HepG2 cells into the posterior side of the right forelimb. Upon reaching a tumor volume of 100 mm^3, the mice were allocated into a control group receiving 9 g/L saline (0.2 mL/d orally), low-dose (L-CB), medium-dose (M-CB), and high-dose (H-CB) CB groups receiving 45.5 mg/(kg/d), 113.75 mg/(kg/d), and 227.5 mg/(kg/d) of CB, respectively, and a sorafenib group administered 20 mg/(kg/d) of sorafenib. Body weight and tumor volume were monitored at 3-d intervals. This study complied with the 1986 Animals (Scientific Procedures) Act of the United Kingdom, ensuring the ethical treatment of laboratory animals. This study was approved by the Ethical Review Committee of Experimental Animal Welfare of the Slacker Jingda Laboratory, Changsha, Hunan, China (Approval No. IACUC-SJA2022105).

Blank and drug-enriched serum preparation: In this study, the rats were allocated to a control group receiving 5 g/L sodium carboxymethyl cellulose and a CB-treated group administered a 157.5 mg/kg CB suspension. Both regimens were administered twice daily for 1 wk. After a fasting period of 12 h, the rats were anesthetized using 30 g/L pentobarbital sodium at a dose of 30 mg/kg to facilitate the subsequent collection of serum.

Network pharmacological analysis

Collection of potential targets and construction of component-target-disease networks: In this study, we identified 22 unique chemicals in CB using UPLC-EIS-Q-TOF-MS analysis. Subsequently, the TCMSP and SwissTargetPrediction tools were employed to predict biological targets, which were further refined using the UniProt database[29]. To identify liver cancer-related targets, a comprehensive search was conducted across multiple databases including DrugBank, OMIM, PharmGKB, and TTD. The obtained data were refined to eliminate redundancy and false positives. Using R software, an intersection analysis was performed between the predicted targets of the bioactive compounds of CB and those present in the liver cancer target database. This enabled us to identify potential therapeutic targets of CB against liver cancer. Finally, a "component-target-disease" interaction network was constructed using Cytoscape.

Protein interaction network construction: A protein-protein interaction (PPI) network for the identified anti-liver cancer targets of CB was established *via* the STRING database. Following this, R software was employed to quantify the frequency of these target interactions, with the results presented in a histogram format for clearer analysis and interpretation.

Analysis of Gene Ontology function and Kyoto Encyclopedia of Genes and Genomes pathway enrichment: The anti-liver cancer targets obtained from CB screening were imported into the Metascape database for Gene Ontology (GO) function analysis. Using R software as a platform, Kyoto Encyclopedia of Genes and Genomes (KEGG) enrichment analysis was performed by inputting the corresponding script commands to clarify the pathways involving the genes.

Molecular docking: To investigate the interactions between liver cancer targets and the active components of CB, we used bioinformatics tools and databases. The structures of the target proteins Wnt5B, β-catenin, and Axin2 were obtained from UniProt. These protein frameworks were prepared for molecular modeling using PyMOL software by removing water molecules and small ligands, and the refined structures were saved in PDB format. The 'component-target-disease' network, focused on 17 primary active components of CB against liver cancer, was explored using PubChem to retrieve the two-dimensional (2D) structures. The chemical structures were further refined and optimized using Chem3D software to ensure accuracy in subsequent studies. Molecular docking simulations were performed using AutoDock Vina software to assess the binding affinity between the CB components and target proteins based on the calculated binding energies. Finally, the results from molecular docking were comprehensively visualized and analyzed using PyMOL software to understand the interactions between the active compounds of CB and the respective liver cancer protein targets.

RNA extraction, RNA sequencing, and bioinformatics analysis

The TRIzol method was used to extract total RNA for quality assessment *via* electrophoresis and bioanalysis. Following RNA extraction, cDNA libraries were sequenced on an Illumina NovaSeq 6000 platform, and reproducibility was evaluated using Pearson's correlation coefficient. RNA expression levels were quantified using Subread software and normalized for gene length and sequencing depth. Differential gene expression analysis was conducted using DESeq2, followed by GO and KEGG pathway enrichment analyses using ClusterProfiler software.

Cell culture

HepG2 cells were cultured in DMEM enriched with 100 mL/L FBS and antibiotic at 37 °C in an atmosphere containing 50 mL/L CO_2, while THP-1 monocytes were similarly cultivated in RPMI-1640. For experimental purposes, PMA was applied at a concentration of 100 ng/mL for 48 h to induce THP-1 monocytes to differentiate into Mφ macrophages. To model tumor-promoting M2 macrophages, these Mφ macrophages were further incubated with IL-4 and IL-13, each at a concentration of 20 ng/mL, for an additional 48 h.

Preparation of conditioned medium

For preparation of Mφ and M2 + 10% (100 mL/L) FBS conditioned media. differentiated Mφ macrophages and M2 macrophages were cultured in DMEM containing 10% (100 mL/L) FBS and 1% (10 mL/L) penicillin-streptomycin. For M2 + 0%, 5%, 10%, and 20% (respectively equal to 0 mL/L, 50 mL/L, 100 mL/L, and 200 mL/L) CB-containing serum (CBS) conditioned media, differentiated M2 macrophages cultured in DMEM were supplemented with 0% (0 mL/L), 5% (50 mL/L), 10% (100 mL/L), and 20% (200 mL/L) CBS and 1% (10 mL/L) penicillin-streptomycin. All the above con-

ditional medium were supernatant collected after culture at 37 ℃ in an atmosphere containing 50 mL/L CO_2 for 24 h.

CCK-8 assay

HepG2 (5×10^5 cells/mL) and THP-1 (2.5×10^4 cells/mL) cells were plated in 96-well plates. After a 24-h cultivation period, media containing various concentrations of CBS (0%, 5%, 10%, and 20%, equal to 0 mL/L, 50 mL/L, 100 mL/L, and 200 mL/L, respectively) were added to the wells for THP-1 cell treatment. HepG2 cells were maintained in different conditioned medium. Cultures were incubated for an additional 24 h to assess the effects of the treatment. Then, 10 μL of CCK-8 solution was added to each well. To facilitate color development, the plates were incubated for an additional 2 h. Optical density was measured at 450 nm using a Spark multimode microplate reader (TECAN, Switzerland).

Flow cytometry

Cell apoptosis detection: HepG2 cells (5×10^5 cells/mL) were inoculated into 96-well plates and incubated for 24 h. Concurrently, THP-1 monocytes, transitioned to Mφ macrophages or subsequently to M2 macrophages, were incubated with either 10% (100 mL/L) control serum or 10% (100 mL/L) CB-enriched serum. Thereafter, the HepG2 cells were treated with media conditioned with these macrophages for an additional day. Following this period, cells were harvested using 800 μL of trypsin without EDTA. Cell apoptosis and viability were analyzed by staining with propidium iodide (5 μL) and annexin V (5 μL). Stained cells were then examined using a CytoFLEX flow cytometer (Beckman, United States).

Macrophage polarization detection: Tumor tissues were minced into small pieces and treated with type I collagenase, then incubated for 1.5 h at 37 °C to facilitate digestion. The cell suspension was gently layered over a density gradient consisting of 300 and 700 mL/L Percoll solutions and centrifuged to separate the lymphocytes, which were harvested from the interface between these two layers. To generate M2-TAMs *in vitro*, cells were dissociated using trypsin without EDTA and collected. Before antibody staining, cells were blocked with anti-mouse CD16/32 antibody (TruStain FcX™) to inhibit non-specific binding, followed by staining with primary antibodies against CD45, CD11b, and F4/80 [all diluted 1:100 in 1% BSA (10 g/L BSA in PBS)] for 30 min at 4 °C. The cells were fixed and permeabilized according to the BD Cytofix/Cytoperm kit protocol, followed by staining with an anti-CD206 antibody for intracellular marker detection. The stained samples were examined using CytoFLEX (Beckman, United States). The data were further evaluated and visualized using FlowJo software (version 10).

Cell scratch assay

HepG2 cells were inoculated into six-well plates, transfected, and subjected to various treatments. After 24 h, a pipette tip was used to draw a straight line across the cell layer and create a scratch to simulate a wound. The wells were then exposed to media supplemented with different concentrations of CB [0% (0 mL/L), 5% (50 mL/L), 10% (100 mL/L), and 20% (200 mL/L)]. Cell migration was monitored and recorded under an inverted microscope at baseline (0 hour) and after 24 h, and the scratch area was quantified using ImageJ software.

Transwell assay

Invasion and migration assays were conducted using 24-well Transwell chambers with 8 μm pores. A mixture of Matrigel and DMEM was placed in the upper chamber containing HepG2 cells, whereas the lower chamber contained DMEM with 100 mL/L FBS as an attractant. After 24 h, non-migrated cells were expunged, whereas migratory cells on the lower surface were fixed, stained, and imaged with ImageJ software to quantify migration and invasion rates.

Real-time reverse transcriptase-polymerase chain reaction

Total RNA was isolated using TRIzol reagent (Vazyme, China) and then reverse-transcribed to cDNA using the All-in-one 1st Strand cDNA Synthesis SuperMix (gDNA Purge). Real-time reverse transcriptase-polymerase chain reaction (RT-qPCR) was conducted using NovoStart® SYBR qPCR SuperMix Plus and the LightCycler® 96™ Real-Time PCR System (Roche Inc., Switzerland). Primers specifically designed for the gene sequences of interest were synthesized based on the sequences available in GenBank (Table 1). The $2^{-\Delta\Delta Ct}$ method was utilized to test the relative expression of each gene.

Western blot analysis

THP-1 monocytes were incubated with 10% (100 mL/L) CB-enriched serum for 24 h and then processed for protein isolation using RIPA buffer (Applygen, China). Protein levels were assessed by the BCA assay, then 50 μg protein samples was separated for Western blot analysis on a 100 mL/L SDS-PAGE gel. The membranes underwent an overnight incubation at 4 °C with primary antibodies targeting Wnt5B, Axin2, β-catenin, and GAPDH, followed by incubation with HRP-conjugated secondary antibodies. Signals were detected using an ECL kit (Biosharp Inc., Anhui, China), followed by imaging using an Amersham Imager 600. Image Pro Plus software was used to conduct band intensity analysis.

Statistical analysis

SPSS version 26.0 was used for statistical analyses. Data normality was verified using the Shapiro-Wilk test. Normally distributed datasets are shown as the mean ± SD. Analysis of variance (ANOVA) was used to evaluate group differences, followed by either SNK post hoc or Tukey's tests, depending on suitability. For two-group comparisons, the independent sample *t* test was applied. The threshold for statistical significance was set at $P < 0.05$.

Table 1 Primers used for qPCR in this study

Gene name	Forward (5' to 3')	Reverse (5' to 3')	Product Length
WNT5B	TCTTCATCCTCCACGGTT	CAGTTTAGGGCTTTCCTGAC	84 bp
β-catenin	CAACTAAACAGGAAGGGATGGAAGG	CAGATGACGAAGAGCACAGATGG	239 bp
AXIN2	TACACTCCTTATTGGGCGATCA	TTGGCTACTCGTAAAGTTTTGGT	151 bp
CCL22	ATCGCCTACAGACTGCACTC	GACGGTAACGGACGTAATCAC	129 bp
TGF-β	GCAGGTATTGATGGCACCTCC	GGCATGCTCCAGCACAGAAG	301 bp
Arg-1	CTTGGCAAAAGACTTATCCTTAG	ATGACATGGACACATAGTACCTTTC	170 bp
IL-10	TTTAAGGGTTACCTGGGTTGC	TTGATGTCTGGGTCTTGGTTC	98 bp
GAPDH	GCTGAGAACGGGAAGCTTGT	GCCAGGGGTGCTAAGCAG	299 bp

RESULTS

Analysis of pharmacodynamic material basis of CB

To examine the pharmacological components of CB, we used UPLC-Q-TOF MS for an extensive analysis. This led to the identification of 22 chemical constituents, including bilirubin, bile acids, cholesterols, and acid esters, as detailed in Table 2 and illustrated in Figure 1. *In vivo* studies revealed 11 components and their metabolites in the blood of rats treated with CB, as shown in Figure 1 and Table 2. Standardized comparisons and quantitative assessments were conducted for the selected components (Figure 1C and Tables 3 and 4). Notably, lithocholic acid was the most abundant component in the CB extract, reaching a concentration of 0.7066 mmol/L, whereas glycohyodeoxycholic acid was the most prevalent in the CB-enriched serum, with a concentration of 0.2759 mmol/L.

CB suppresses liver cancer growth in vivo

The anti-tumor effects of CB have been previously evaluated in animal models. Treatment with low, medium, and high doses of CB (L-CB, M-CB, and H-CB) and sorafenib significantly reduced both the size and weight of the tumors relative to the controls (Figure 2A-C). Interestingly, there was no notable impact on the body weight of the mice across all experimental groups (Figure 2D).

The anti-cancer efficacy of CB was further validated by histological analysis. As illustrated in Figure 2E, hematoxylin and eosin staining of tumor tissue revealed distinct morphological indications of tumor regression following treatment with medium and high doses of CB and sorafenib. The observed signs of regression include degenerative changes in tumor cells, reduced nucleolar staining intensity, and the presence of nuclear fragments, which are indicative of diminished malignancy post-treatment. These findings suggest that CB, particularly at medium and high doses, significantly impedes the growth of liver cancer.

Cyberpharmacology analysis of CB components for anti-liver cancer study utilizing UPLC-Q-TOF MS

Construction of a "component-target-disease" network: Following database searching, 392 possible chemical targets associated with the components of CB were discovered. Liver cancer-related targets were compiled from comprehensive databases, including DrugBank, OMIM, PharmGKB, and TTD, resulting in 6307 targets associated with liver cancer. Using R software for data analysis, we matched the targets related to the active components of CB against those associated with liver cancer. This comparative approach led to the identification of 168 potential anti-liver cancer targets using intersection analysis (Figure 3A). The constructed component-target-disease interaction network (Figure 3B) visualized the potential efficacy of CB against liver cancer, encompassing 463 edges and 184 nodes, with an average degree value of 5.04. Notably, compounds such as gelsevirine, nisinic acid, methyl cholate, 7-ketolithocholic acid, glycocholic acid, deoxyloganin, bilirubin, hyodeoxycholic acid, campechic acid A, glycohyodeoxycholic acid, and phorbol 12,13-dimyristate were identified with degree values ≥ 10, highlighting their significant role in the anti-liver cancer activity of CB[30].

GO analysis: We used PPI network analysis to identify the primary targets of CB in liver cancer. This analysis revealed TNF and IL-6 as central targets (Figure 3C), highlighting their significant roles in the immune response associated with liver cancer. Furthermore, GO functional analysis was conducted on these key targets to categorize their roles in biological processes, molecular functions, and cellular components. The top 20 items were statistically significant ($P < 0.01$; Figure 3D). Our findings demonstrate that the biological processes involved in liver cancer pathogenesis mainly include the regulation of the MAPK cascade signaling pathway, hormonal responses, positive regulation of cell migration and death, and secretory regulation. The cellular components associated with the pathogenesis of liver cancer predominantly comprise membrane rafts, receptor complexes, postsynaptic membranes, and cellular projection membranes.

KEGG analysis: Moreover, the core targets were analyzed, and the signaling pathways with $P < 0.01$ were chosen for visualization (Figure 3E). KEGG analysis revealed significant pathways, including the PI3K-Akt, Wnt, Rap1, and Ras pathways (Figure 3E). The Wnt pathway, which is involved in cell proliferation, differentiation, and apoptosis, has been

Table 2 Information analysis of 22 compounds in *Calculus bovis*

Number	Retention time (min)	Molecular weight	Molecular formula	Name	Serum
1	11.362	222.0905	C13H10N4	1,5-Diphenyltetrazole	√
2	13.144	374.1593	C17H26O9	Deoxyloganin	
3	14.277	352.1787	C21H24N2O3	Gelsevirine	√
4	16.133	678.5017	C40H70O8	Campechic acid A	
5	16.381	190.1205	C6H13NO6	D-Glucosaminic Acid	√
6	18.253	221.0953	C14H11N3	Isoquinoline	
7	21.631	515.2957	C26H45NO7S	Taurocholic acid	
8	22.525	408.2876	C24H40O5	Cholic acid	√
9	23.039	584.2634	C33H36N4O6	Bilirubin	√
10	23.716	465.309	C26H43NO6	Glycocholic acid	√
11	24.844	499.2968	C26H45NO6S	Taurodeoxycholic acid	√
12	25.939	256.2402	C16H32O2	Palmitic acid	
8	26.684	408.2876	C24H40O5	Cholic acid	
13	27.776	449.3141	C26H43NO5	Glycohyodeoxycholic acid	√
14	28.919	392.2927	C24H40O4	Hyodeoxycholic acid	√
15	29.765	390.277	C24H38O4	7-Ketolithocholic acid	
16	31.405	356.2715	C24H40O4	Anoxycholic acid	
17	32.051	784.5853	C24H40O4	Deoxycholic acid	
18	33.541	222.162	C14H22O2	Isobornyl methacrylate	
19	37.532	422.3032	C25H42O5	Methyl cholate	
20	37.556	280.2402	C24H40O3	Lithocholic acid	√
21	37.701	148.016	C8H4O3	Isobenzofuran-1,3-dione	
22	38.046	304.2402	C20H32O2	Arachidonic acid	√

Table 3 Quantitative analysis of active components in *Calculus bovis* extract

No.	Component	Concentration of standard	Peak area of standard	Peak area of sample	Concentration of sample (mM)
1	Cholic acid	1 mg/mL	303383832.9	111239787.3	0.366663531
2	Glycohyodeoxycholic acid	1 mg/mL	263903105.5	151518620.6	0.574144894
3	Anoxycholic acid	1 mg/mL	255212724.5	84507042.75	0.331123939
4	Deoxycholic acid	1 mg/mL	303655598.9	116148310.7	0.382500145
5	Lithocholic acid	1 mg/mL	377852336.8	133498724.1	0.706618491

Table 4 Quantitative analysis of active components in *Calculus bovis*-enriched serum

No.	Component	Concentration of standard	Peak area of standard	Peak area of sample	Concentration of sample (mM)
1	Cholic acid	1 mg/mL	18294415.89	4577619.85	0.250219514
2	Glycohyodeoxycholic acid	1 mg/mL	14604541.97	4029834.55	0.275930225
3	Lithocholic acid	1 mg/mL	15655005.77	175178.8	0.022379909

A

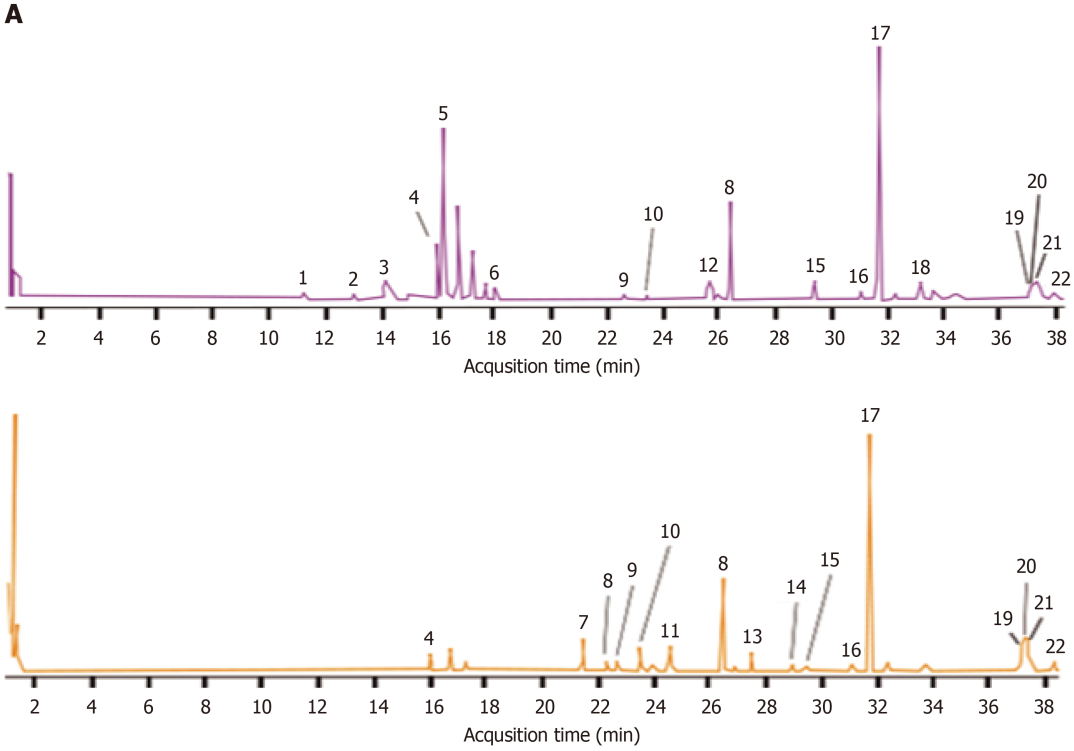
Acqusition time (min)
Acqusition time (min)

B

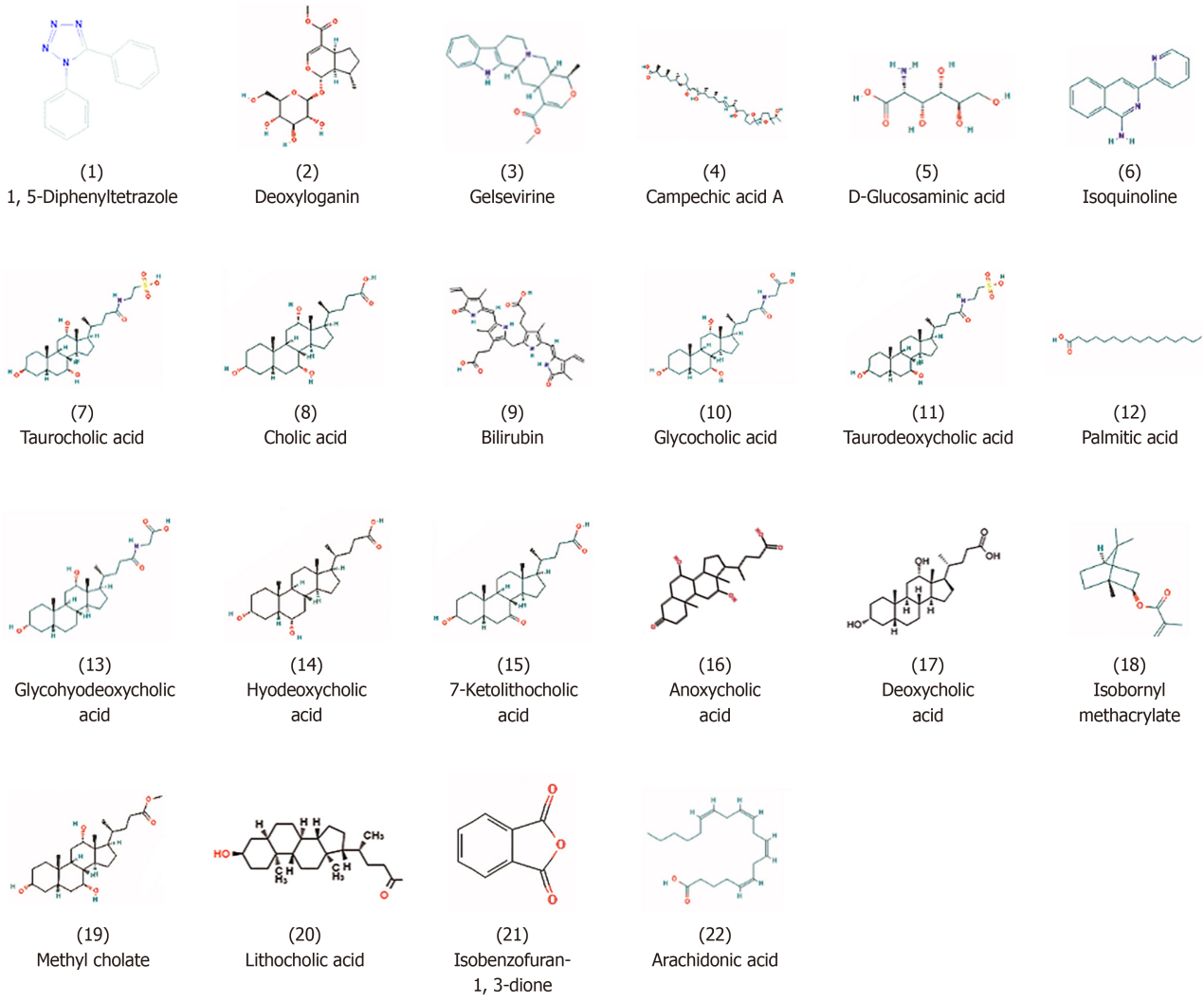
(1) 1, 5-Diphenyltetrazole
(2) Deoxyloganin
(3) Gelsevirine
(4) Campechic acid A
(5) D-Glucosaminic acid
(6) Isoquinoline
(7) Taurocholic acid
(8) Cholic acid
(9) Bilirubin
(10) Glycocholic acid
(11) Taurodeoxycholic acid
(12) Palmitic acid
(13) Glycohyodeoxycholic acid
(14) Hyodeoxycholic acid
(15) 7-Ketolithocholic acid
(16) Anoxycholic acid
(17) Deoxycholic acid
(18) Isobornyl methacrylate
(19) Methyl cholate
(20) Lithocholic acid
(21) Isobenzofuran-1, 3-dione
(22) Arachidonic acid

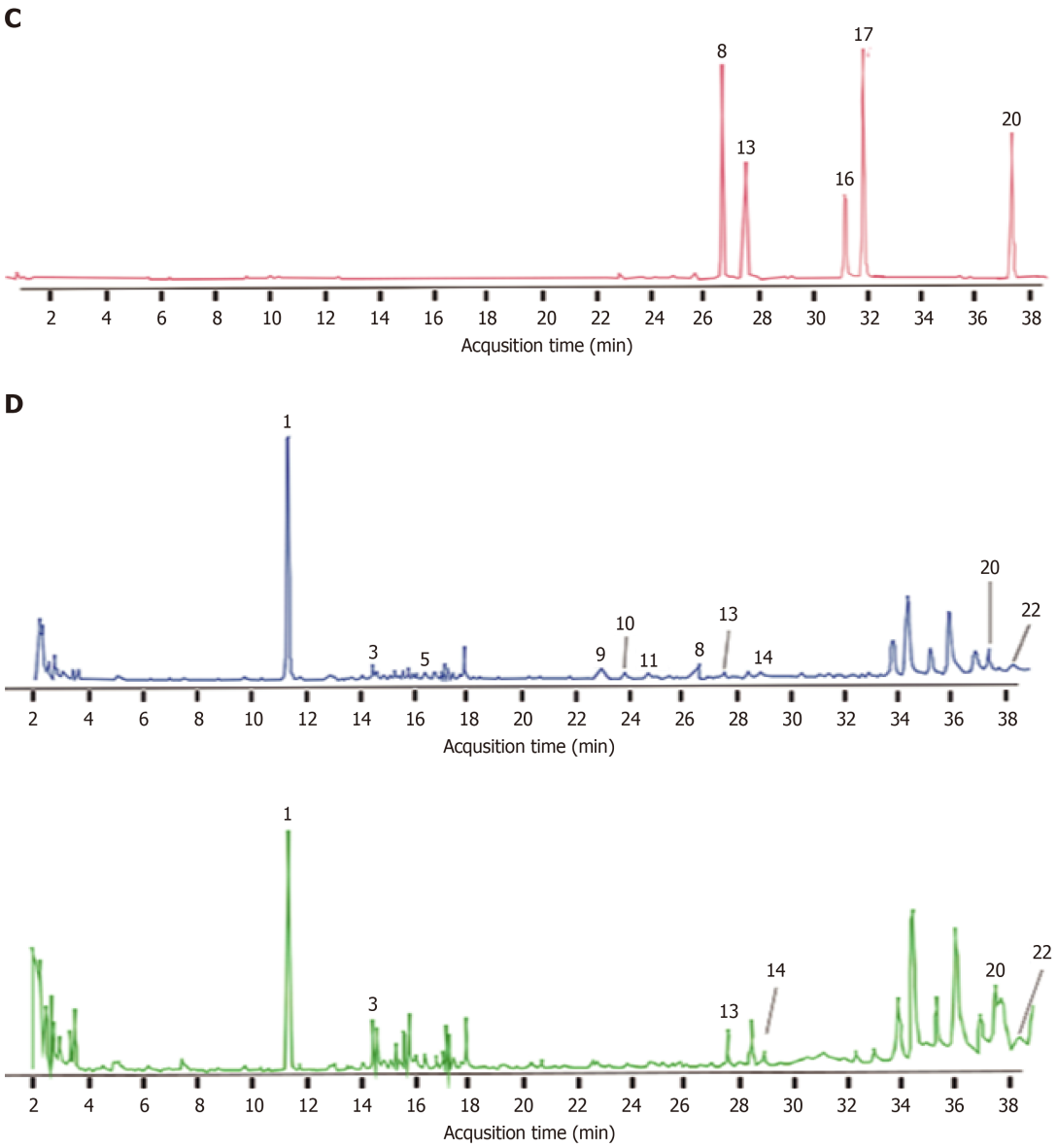

Figure 1 Analysis of pharmacodynamic material basis of *Calculus bovis*. A: Positive and negative ion chromatograms of *Calculus bovis* (CB) extract; B: Structural diagrams of 22 components of CB; C: Ion chromatogram of the standardized substances of CB extract; D: Ion chromatograms of CB-enriched serum and blank serum.

linked to cancer progression and immune system modulation. Based on these insights, further detailed investigation into the Wnt pathway was prioritized to better understand the mechanism of action of CB against liver cancer, supported by the findings of Pai *et al*[31].

Molecular docking results: The study excluded isolinolic acid from further analysis owing to the absence of a 2D structure in the database. To investigate the interactions between the target proteins associated with the Wnt signaling pathway and the active components of CB, molecular docking was conducted on the remaining 16 active components, including Wnt5B, β-catenin, and Axin2. A binding energy threshold of -5.0 kcal/mol was set as an indicator of strong affinity between the active ingredients and their target proteins. Our findings revealed that bilirubin and bile acid-like compounds such as glycocholic acid, taurodeoxycholic acid, glycohyodeoxycholic acid, hyodeoxycholic acid, and 7-ketolithocholic acid exhibited binding energies ≤ -6.5 kcal/mol with Wnt5B, β-catenin, and Axin2 proteins. This is depicted in Figure 3F and G, which demonstrate a stable binding conformation. These results suggest that CB inhibits liver cancer progression by modulating the Wnt signaling pathway.

Wnt pathway and its target molecules are involved in the effects of CB on M2-TAM

Transcriptome analysis was performed to investigate the effects of CB on gene functionality during cell migration. This analysis identified significant changes in 820 genes, including 359 genes with increased expression and 461 genes with decreased expression (Figure 4A). GO and KEGG enrichment analyses were then performed on differentially expressed genes, which indicated that the Wnt pathway is a key target of CB-mediated inhibition in liver cancer. Furthermore, CB

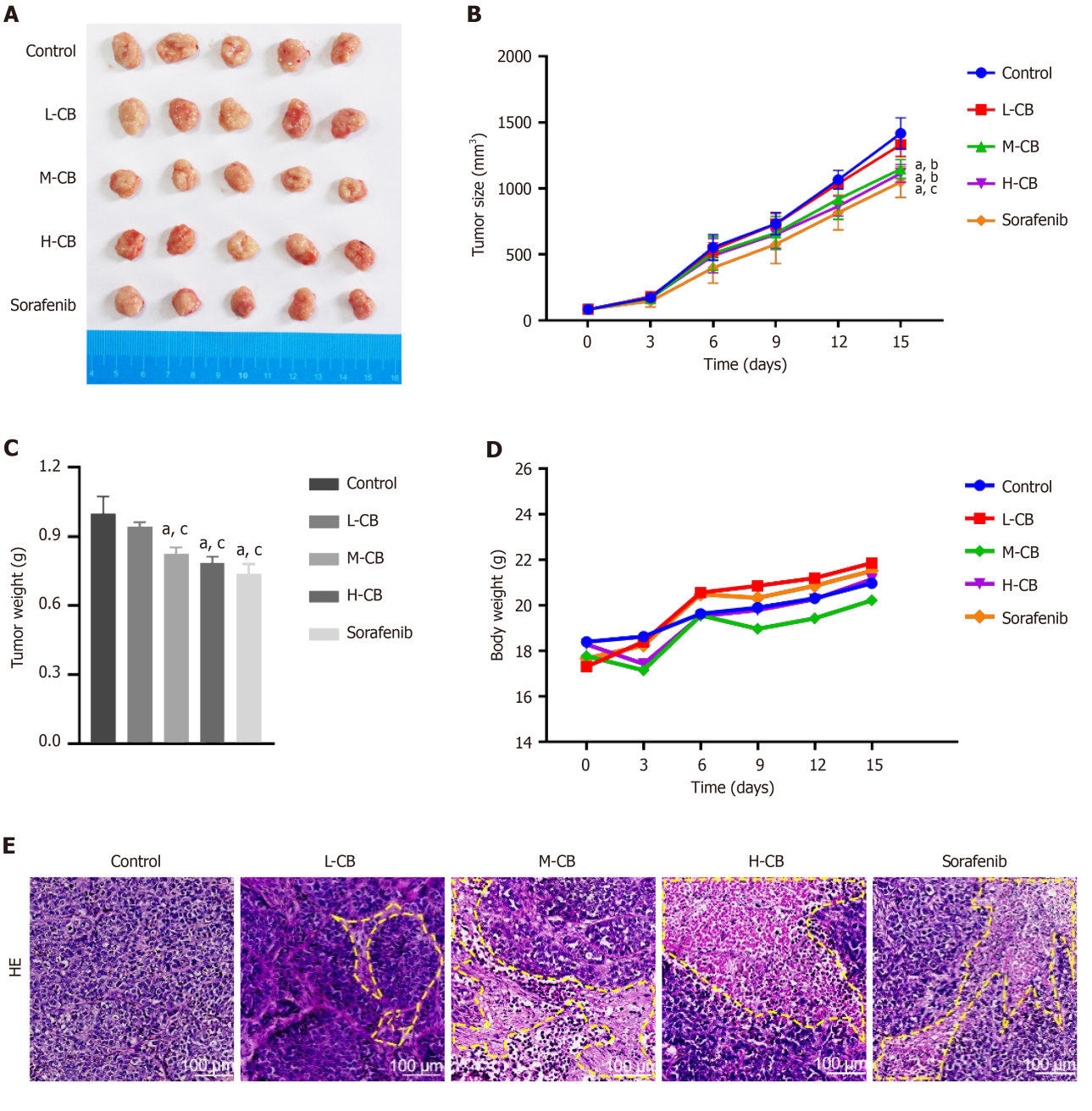

Figure 2 *In vivo* anti-tumor activity of *Calculus bovis*. A: Pictures of tumors in each group after treatment; B: Tumor size changes in each group during treatment; C: Tumor weight of each group during treatment; D: Changes in weight of mice in each group during treatment; E: Hematoxylin-eosin staining results of tumor tissue sections in each group after treatment. Control: Model group. CB: *Calculus bovis*; L-CB: Low-dose CB group; M-CB: Medium-dose CB group; H-CB: High-dose CB group; Differences were assessed using one-way ANOVA and multiple comparisons were determined using Tukey's test. $^{a}P < 0.01$ *vs* control, $^{b}P < 0.05$ *vs* L-CB, $^{c}P < 0.01$ *vs* L-CB.

appeared to affect differential mRNA expression in mouse tumor tissues by targeting molecular functions and biological processes related to the Wnt pathway (Figure 4B-D). Notably, among the genes in this pathway, *CCL22* and *TGF-β*, both known for their association with M2-TAM polarization, were significantly enriched. Therefore, our results support the hypothesis that CB exerts its anti-liver cancer effects through modulation of the Wnt pathway and subsequent alteration of M2-TAM polarization.

CBS inhibits M2 macrophage polarization in vitro

To assess the cytotoxic effects of CBS on THP-1 cells, we initially performed a CCK-8 assay using varying concentrations of CBS [5% (50 mL/L), 10% (100 mL/L), and 20% (200 mL/L]). Figure 5A shows no significant effects on cell viability after exposure to CBS. Subsequently, we investigated the ability of CBS to inhibit M2 macrophage polarization stimulated by IL-13 and IL-4. Flow cytometry was used to measure CD86 and CD206 surface markers on THP-1 cells. As shown in Figure 5B, stimulation with IL-13 and IL-4 resulted in substantial upregulation of CD206 expression, confirming successful M2-TAM polarization. Furthermore, we evaluated the influence of different concentrations of BS and CBS on the mRNA expression of *CD206* in M2-TAM using RT-qPCR. Across the BS concentrations, CD206 expression remained

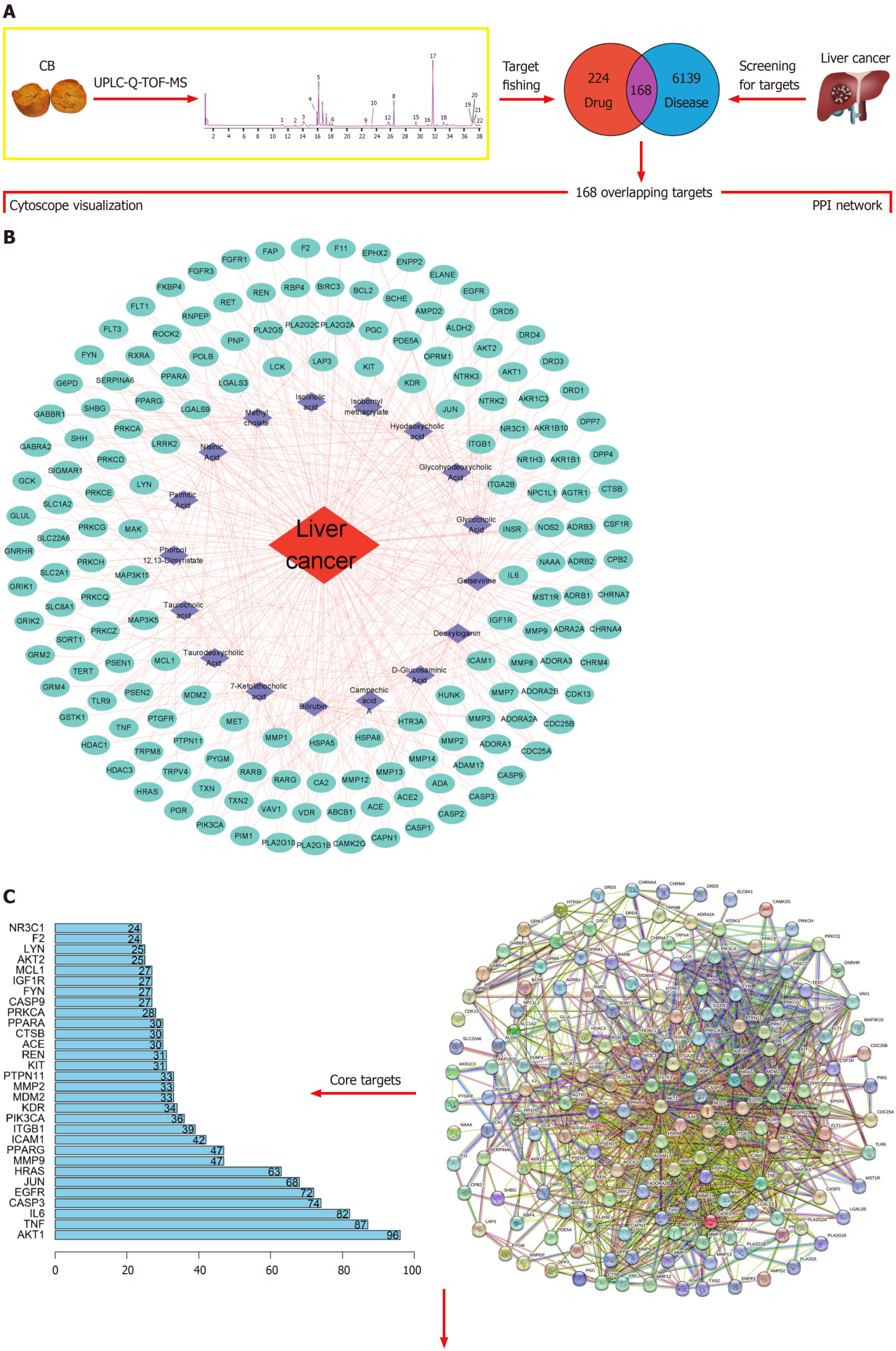
A
CB
UPLC-Q-TOF-MS
Target fishing
224 Drug
168
6139 Disease
Screening for targets
Liver cancer
168 overlapping targets
Cytoscope visualization
PPI network
B
Liver cancer
C
Core targets
NR3C1 24
F2 24
LYN 25
AKT2 25
MCL1 27
IGF1R 27
FYN 27
CASP9 27
PRKCA 28
PPARA 30
CTSB 30
ACE 30
REN 31
KIT 31
PTPN11 33
MMP2 33
MDM2 33
KDR 34
PIK3CA 36
ITGB1 39
ICAM1 42
PPARG 47
MMP9 47
HRAS 63
JUN 68
EGFR 72
CASP3 74
IL6 82
TNF 87
AKT1 96
0
20
40
60
80
100

D

GO annotation

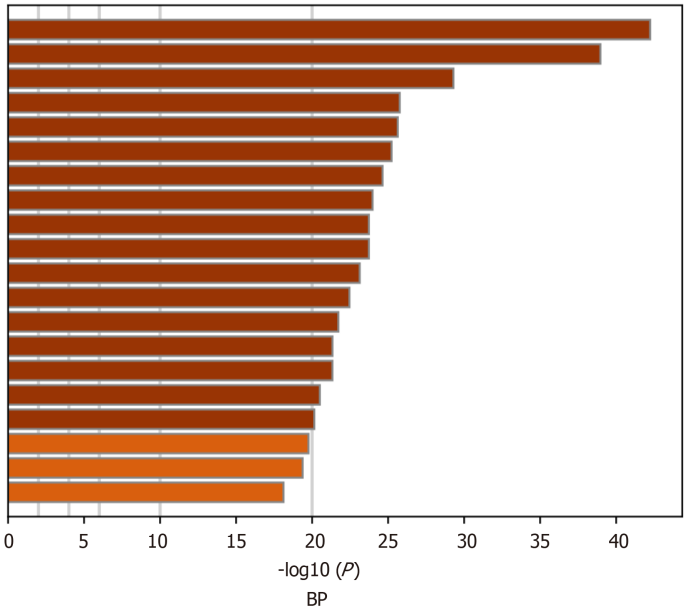

GO:0043408: Regulation of MAPK cascade
GO:0009725: Response to hormone
GO:0030335: Positive regulation of cell migration
GO:0010942: Positive regulation of cell death
GO:0051046: Regulation of secretion
G0:0044057: Regulation of system process
GO:0043269: Regulation of ion transport
GO:0071407: Cellular response to organic cyclic compound
GO:0009611: Response to wounding
GO:0050804: Modulation of chemical synaptic transmission
GO:0032103: Positive regulation of response to external stimulus
GO:0070201: Regulation of establishment of protein localization
GO:0030155: Regulation of cell adhesion
GO:0010035: Response to inorganic substance
GO:0009991: Response to extracellular stimulus
GO:0070482: Response to oxygen levels
GO:0009410: Response to xenobiotic stimulus
GO:0010817: Regulation of hormone levels
GO:1901214: Regulation of neuron death
GO:0009314: Response to radiation

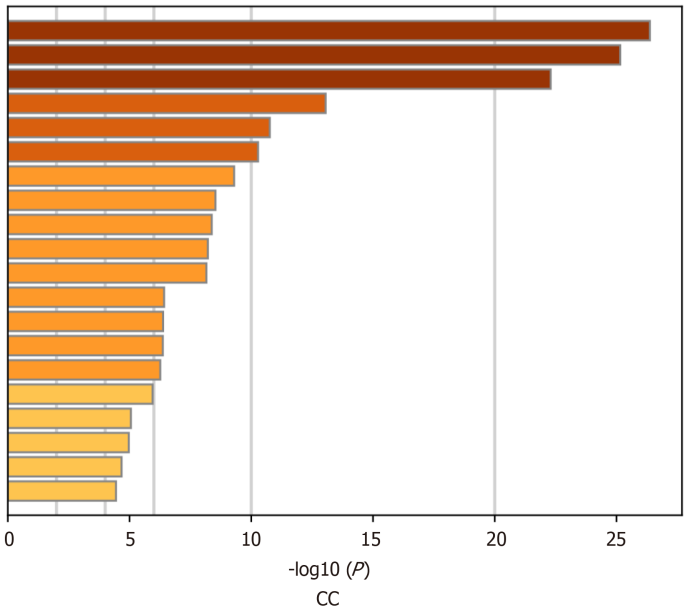

GO:0045121: Membrane raft
GO:0043235: Receptor complex
GO:0098794: Postsynapse
GO:0031253: Cell projection membrane
GO:0098552: Side of membrane
GO:0048471: Perinuclear region of cytoplasm
GO:0000323: Lytic vacuole
GO:0045177: Apical part of cell
GO:0032589: Neuron projection membrane
GO:0031012: Extracellular matrix
GO:0030139: Endocytic vesicle
GO:0098982: GABA-ergic synapse
GO:0098685: Schaffer collateral - CA1 synapse
GO:0043209: Myelin sheath
GO:0042470: Melanosome
GO:0030673: Axolemma
GO:0044853: Plasma membrane raft
GO:0045178: Basal part of cell
GO:0099523: Presynaptic cytosol
GO:0005788: Endoplasmic reticulum lumen

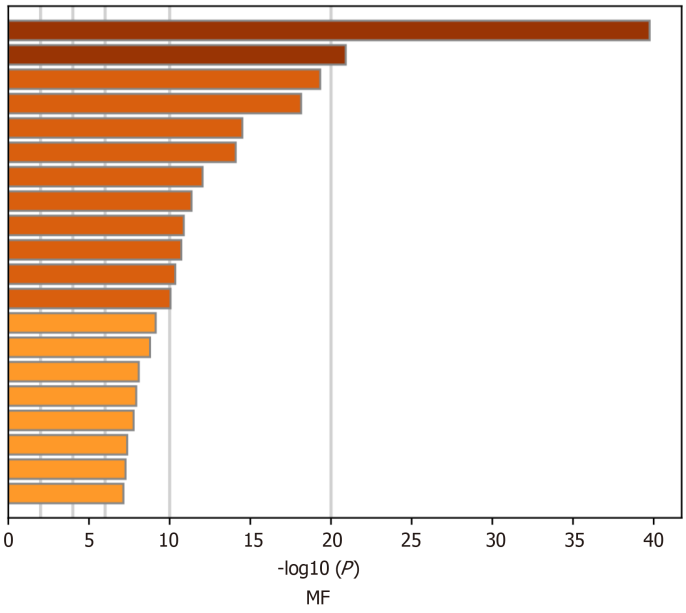

GO:0004712: protein serine/threonine/tyrosine kinase activity
GO:0004713: protein tyrosine kinase activity
GO:0008233: peptidase activity
GO:0030594: neurotransmitter receptor activity
GO:1901338: catecholamine binding
GO:0019904: protein domain specific binding
GO:0019900: kinase binding
GO:0004698: calcium-dependent protein kinase C activity
GO:0043560: insulin receptor substrate binding
GO:0042803: protein homodimerization activity
GO:0004879: nuclear receptor activity
GO:0002020: protease binding
GO:0008238: exopeptidase activity
GO:0051380: norepinephrine binding
GO:0001609: G protein-coupled adenosine receptor activity
GO:0008134: transcription factor binding
GO:0004190: aspartic-type endopeptidase activity
GO:0047498: calcium-dependent phospholipase A2 activity
GO:0019902: phosphatase binding
GO:0005178: integrin binding

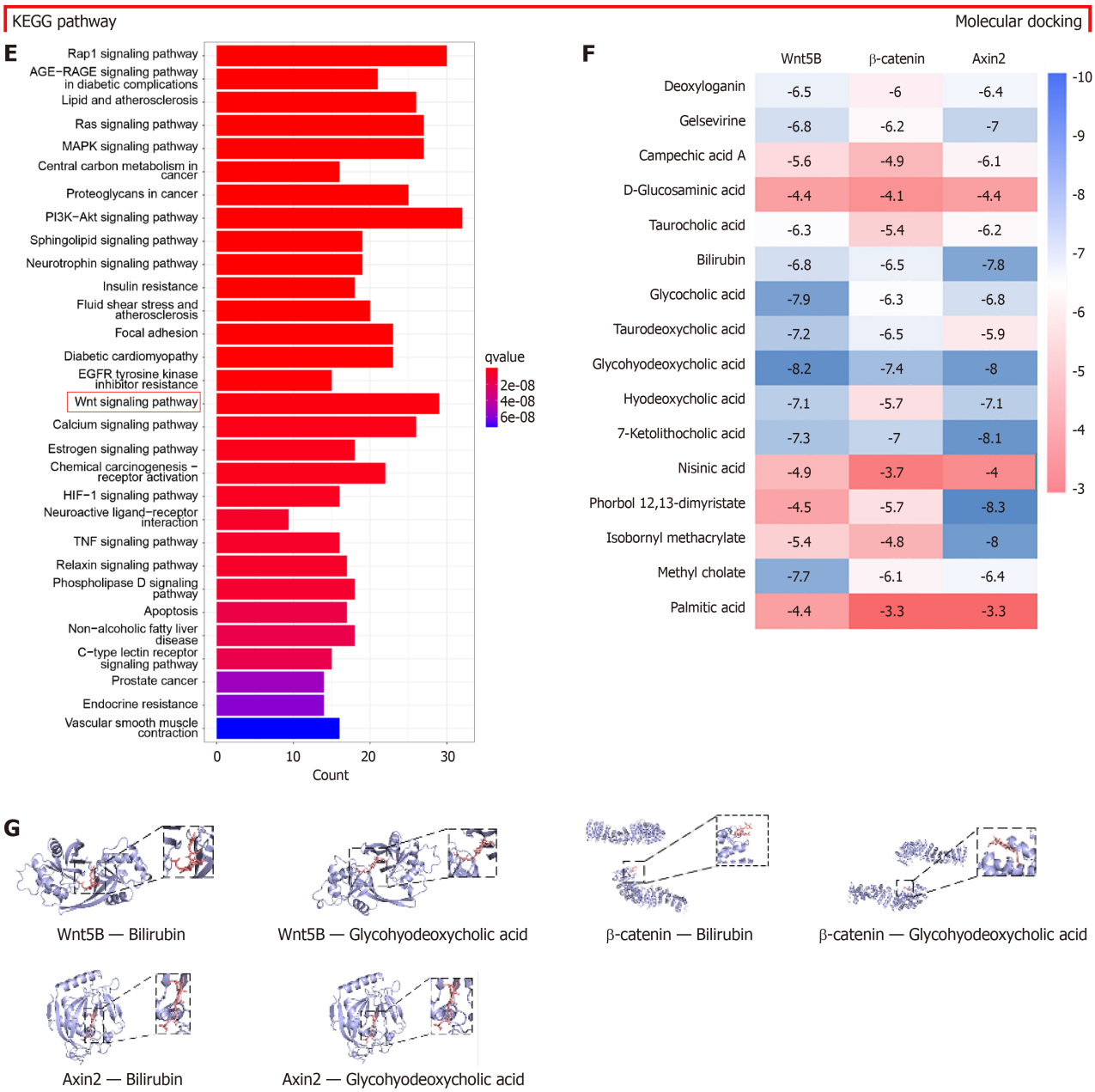

Figure 3 Cyberpharmacological study on anti-liver cancer mechanism of active components of *Calculus bovis* based on UPLC-Q-TOF-MS analysis. A: Intersection plot of potential targets of *Calculus bovis* (CB) and liver cancer targets; B: Component-target-disease interaction network of CB against liver cancer. The purple quadrilaterals represent the active components of CB; C: Protein-protein interaction network; D: Gene Ontology function analysis of CB against liver cancer; E: Kyoto Encyclopedia of Genes and Genomes pathway enrichment analysis of CB against liver cancer; F: Minimum binding energy of the active components of CB with core target proteins; G: Molecular docking diagram of some active components.

stable, with no significant alterations. However, notable differences in *CD206* mRNA expression were detected when comparing the groups treated with 10% (100 mL/L) CBS to those receiving 10% (100 mL/L) BS, as well as between the 20% (200 mL/L) CBS group and the corresponding BS group ($P < 0.01$). Treatment with both 10% and 20% (100 and 200 mL/L) CBS led to a statistically significant downregulation of *CD206* mRNA expression compared to treatment with 5% (50 mL/L) CBS; however, there was no significant difference between these two higher concentrations (Figure 5C). Consequently, 10% CBS (100 mL/L) was selected for subsequent experiments. Flow cytometry analysis demonstrated that treatment with this concentration effectively reduced CD206 expression in M2-TAM cells (Figure 5D). Additionally, RT-qPCR analysis revealed significant reductions in mRNA levels of *CCL22*, *Arg-1*, *TGF-β2*, and *IL-10* (Figure 5E). Collectively, these findings indicate that CBS effectively inhibits M2-TAM polarization.

CBS mitigates the proliferative and migratory properties of liver cancer cells by suppressing TAM polarization to M2

We used the CCK-8 assay to evaluate the effects of various concentrations of CBS on HepG2 cell proliferation in a medium conditioned with M2 macrophages, which revealed notable inhibitory effects (Figure 6A). Flow cytometry analysis indicated an enhancement in the proliferation of liver cancer cells compared to Mφ macrophages. Notably, enhanced apoptosis was observed in the group treated with M2 + 10% (100 mL/L) CBS conditioned medium, in stark

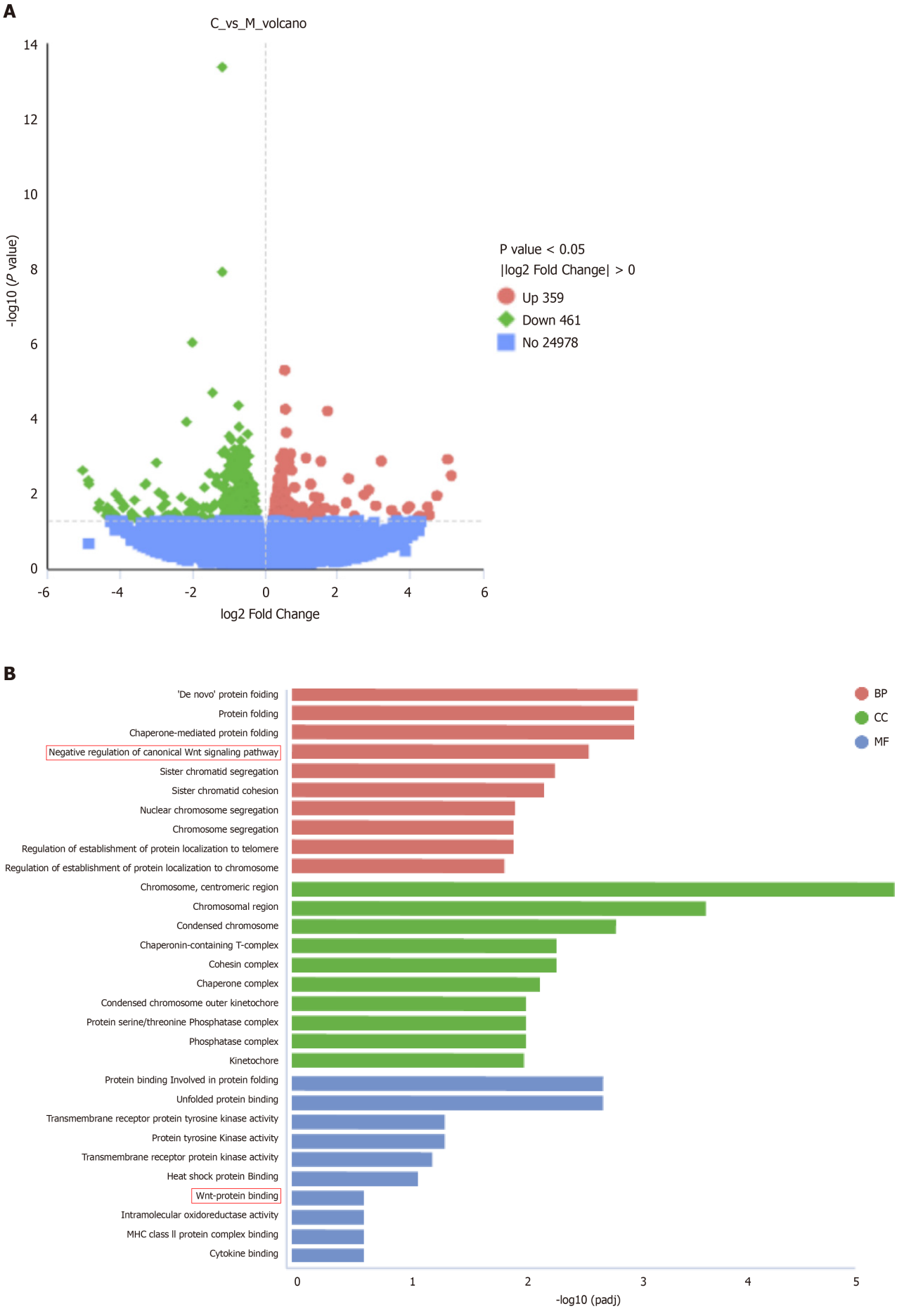
A
C_vs_M_volcano
-log10 (P value)
log2 Fold Change
P value < 0.05
|log2 Fold Change| > 0
Up 359
Down 461
No 24978
B
'De novo' protein folding
Protein folding
Chaperone-mediated protein folding
Negative regulation of canonical Wnt signaling pathway
Sister chromatid segregation
Sister chromatid cohesion
Nuclear chromosome segregation
Chromosome segregation
Regulation of establishment of protein localization to telomere
Regulation of establishment of protein localization to chromosome
Chromosome, centromeric region
Chromosomal region
Condensed chromosome
Chaperonin-containing T-complex
Cohesin complex
Chaperone complex
Condensed chromosome outer kinetochore
Protein serine/threonine Phosphatase complex
Phosphatase complex
Kinetochore
Protein binding Involved in protein folding
Unfolded protein binding
Transmembrane receptor protein tyrosine kinase activity
Protein tyrosine Kinase activity
Transmembrane receptor protein kinase activity
Heat shock protein Binding
Wnt-protein binding
Intramolecular oxidoreductase activity
MHC class II protein complex binding
Cytokine binding
BP
CC
MF
-log10 (padj)

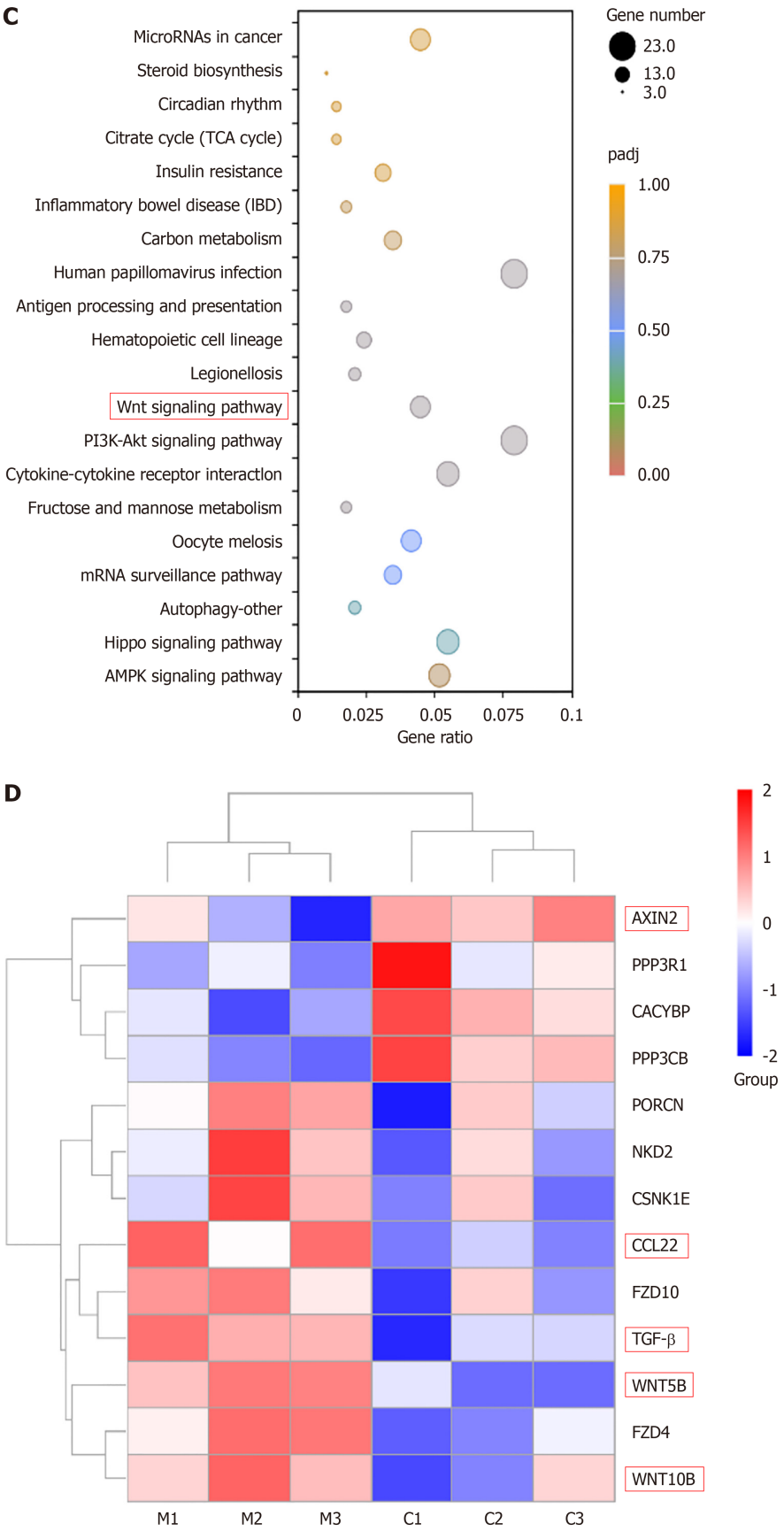

Figure 4 Differentially expressed genes between *Calculus bovis*-treated group and control group ($q < 0.05$ and log2FlodChange > 0) after transcriptome sequences were analyzed by bioinformatics. A: Differential gene volcano plot between the *Calculus bovis* (CB)-treated and control groups; B: Histogram of Gene Ontology enrichment results of differentially expressed mRNAs in the CB-treated and control groups (top 10); C: Bubble plots of Kyoto Encyclopedia of Genes and Genomes enrichment results of differentially expressed mRNAs in the CB-treated and control groups (top 20); D: Heatmap of selected genes involved in the Wnt pathway.

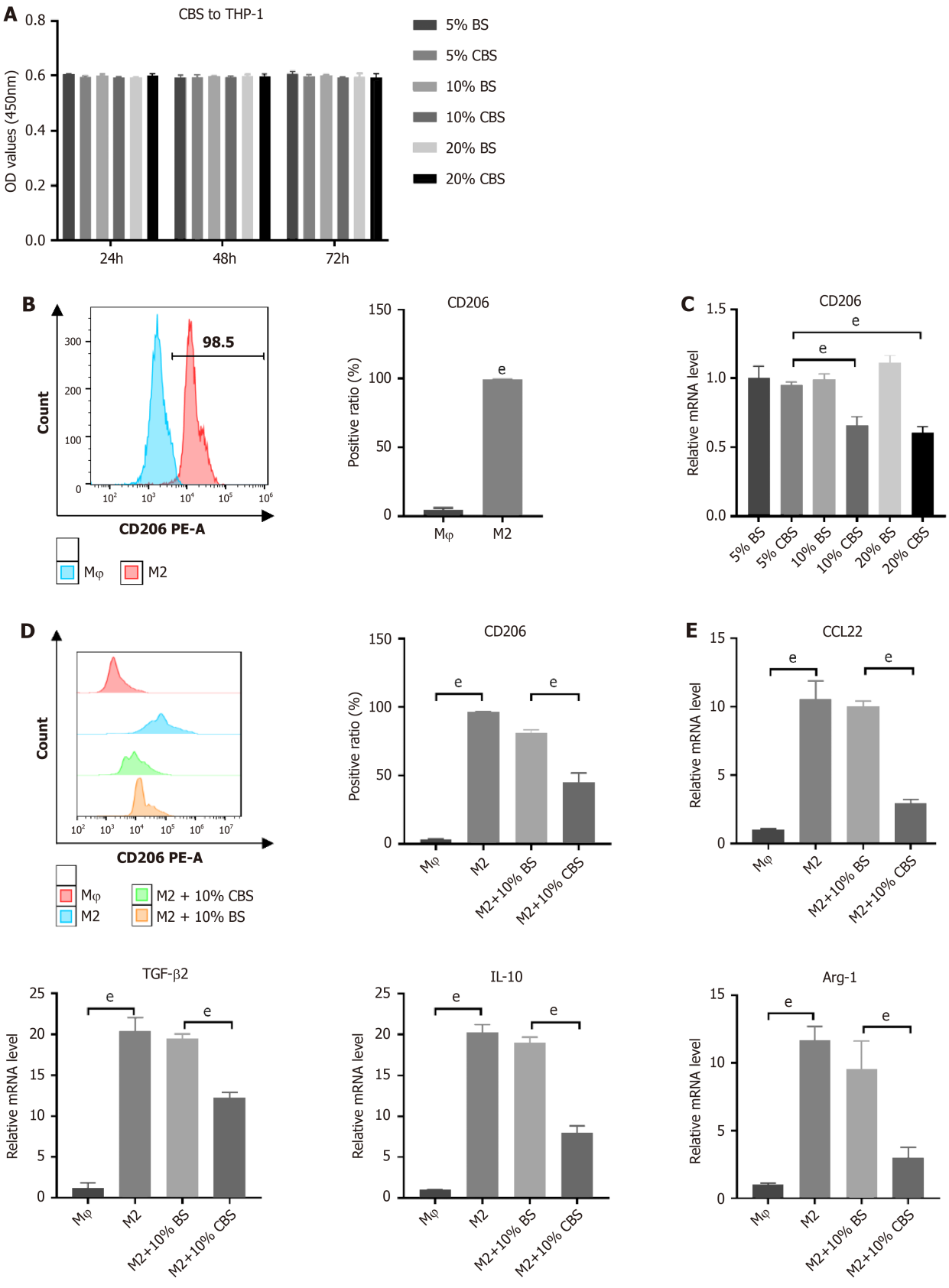

Figure 5 *Calculus bovis*-enriched serum inhibits polarization of M2 tumor-associated macrophages. A: Cytotoxicity of *Calculus bovis*-enriched serum (CBS) on THP-1 cells by Cell Counting Kit-8 assay. The blank group served as a control; B: CD206 quantification in THP-1 cells after IL-4 and IL-13 induction by flow cytometry; C: The mRNA expression levels of *CD206* after intervention of M2 tumor-associated macrophages (M2-TAMs) with different concentrations of blank serum and CBS; D: Quantification of CD206 in M2-TAMs after 10% (100 mL/L) CBS intervention by flow cytometry; E: The mRNA expression levels of *CCL22, TGF-β2, IL-10*, and *Arg-1* after 10% (100 mL/L) CBS intervention in M2-TAMs. $^{d}P < 0.05$, $^{e}P < 0.01$. BS: Blank serum; CBS: CB-enriched serum.

contrast to the Mφ + 10% (100 mL/L) BS and M2 + 10% (100 mL/L) BS conditioned medium groups (Figure 6B). These results confirm that CBS not only impedes M2-TAM-induced proliferation of liver cancer cells but also significantly promotes their apoptosis. In the 24-h wound healing assay, the migratory capacity of HepG2 cells was increased when cultured with medium from the M2 + 10% (100 mL/L) BS group, compared to the Mφ + 10% (100 mL/L) BS group. However, this enhanced migratory behavior was significantly reduced following treatment with M2 + 10% (100 mL/L) CBS-conditioned medium (Figure 6C). Similarly, the Transwell invasion assay revealed that M2 + 10% (100 mL/L) CBS-conditioned medium effectively decreased the migration rate of HepG2 cells (Figure 6D). Collectively, these findings indicate that CBS-treated M2-TAM medium considerably diminishes the cell invasion and migration capabilities of liver cancer, underscoring the potential therapeutic value of CB in halting liver cancer progression.

CBS inhibits M2-TAM polarization through the Wnt pathway

RT-qPCR and Western blot analysis showed upregulated expression of Wnt5B and β-catenin, along with a reduction in Axin2 levels, confirming the activation of the Wnt pathway (Figure 7A and B). Significantly, the inclusion of 10% (100 mL/L) CBS markedly mitigated IL-13/IL-4 induced alterations, suggesting that Wnt pathway modulation occurred in the CBS-mediated inhibition of macrophage M2 polarization. To further elucidate the effect of CBS on Wnt signaling in macrophages, we used SKL2001, a recognized activator of this pathway, in our experimental design. As depicted in Figure 7C, THP-1 cells co-treated with 10% (100 mL/L) CBS and SKL2001 showed a significant elevation in β-catenin levels compared with cells treated with 10% (100 mL/L) CBS alone. Additionally, flow cytometry analysis demonstrated that treatment with 10% (100 mL/L) CBS reduced CD206 expression by approximately 40%. Notably, simultaneous administration of SKL2001 and CBS abrogated the CBS-induced suppression of CD206 expression (Figure 7D). These findings highlight that the inhibitory effect of CBS on M2-TAM polarization predominantly operates through the downregulation of the Wnt pathway.

CB regulates M2 polarization via the Wnt pathway in vivo to combat liver cancer

In the subsequent *in vivo* experiments, we aimed to confirm the effects of the Wnt pathway. Consistent with our earlier findings, CB treatment resulted in significant downregulation of Wnt5B and β-catenin, alongside increased expression of Axin2 (Figure 8A and B). These findings suggest that CB suppresses Wnt pathway activity. Moreover, flow cytometry analysis indicated that CB effectively reduced the expression of the M2 macrophage marker CD206, with the most significant decrease observed in the high-dose group (Figure 8C).

DISCUSSION

Despite recent advances in treatment methods that have reduced liver cancer mortality, prognosis remains poor owing to high rates of metastasis and chemotherapy resistance. TCM can inhibit liver cancer by regulating the TME, thus providing a new perspective on liver cancer treatment. CB, a classic herb in TCM described in ancient medical texts and with thousands of years of use, is a foundational substance in compound formulations such as Xihuang Pills and Pien Tze Huang, used for treating tumors. Its immunomodulatory and anti-inflammatory effects are well documented, highlighting its medicinal significance in traditional Chinese therapeutic practices[32-34]. We hypothesized that CB inhibits tumor progression by modulating macrophages within the TME, and subsequently investigated this effect.

Antitumor experiments conducted *in vivo* and *in vitro* have demonstrated that CB significantly inhibits the progression of liver cancer. Network pharmacology and transcriptome sequencing analysis indicated enrichment of the Wnt/β-catenin signaling pathway, suggesting that the mechanism of action of CB may involve this pathway. Previous studies have established that the Wnt signaling pathway is crucial for the pathogenesis of liver cancer[35-37], as it regulates the proliferation of liver cancer stem cells and promotes tumor growth. Our research illustrated the mechanism that CB impedes progression of liver cancer by alerting M2-TAM polarization *via* Wnt/β-catenin pathway modulation. Detailed serum analysis revealed 11 bioactive compounds, including bilirubin, which exhibits antioxidant, anticancer, and anti-inflammatory effects as documented by Yu *et al*[26]. Bile acid-like components and acid esters, which are recognized for their roles in enterohepatic circulation and their antitumor properties[38], also contribute to the hepatoprotective profile of CB. These findings verify the multiple therapeutic effects of CB in targeting liver cancer through the interaction of its active constituents.

In the further analysis of the Wnt pathway, a significant upregulation of CCL22 and TGF-β2 was observed among downstream molecules. The stimulation of TGF-β and Wnt/β-catenin pathways is known to facilitate M2 macrophage polarization, which has a significant impact in connecting inflammatory and oncogenic processes. This polarization further enhances the invasion and migration of liver cancer[39]. It has been demonstrated that CCL22 exacerbates autoimmune diseases by recruiting macrophages and enhancing their effector functions. Neutralizing CCL22 leads to an altered cytokine profile within macrophages, characterized by reduced TNF-α levels and increased IL-10 levels, aligning with the characteristics of M2-TAMs[17,40]. CB may impede liver cancer progression by obstructing M2-TAM polarization *via* the Wnt/β-catenin pathway. *In vitro*, CB-supplemented serum reduced M2-TAM markers and cytokines in THP-1 cells activated with IL-4/IL-13 for 24 h. Identification of M2-TAMs relies on their responsiveness to IL-4, IL-10, IL-13, and TGF-β, resulting in elevated levels of CD206 and Arg-1 expression[41]. Moreover, TAMs tend to secrete lower amounts of TNF-α and IL-1β while exhibiting higher concentrations of TGF-β and IL-10[41-43]. These observations support the findings of this study.

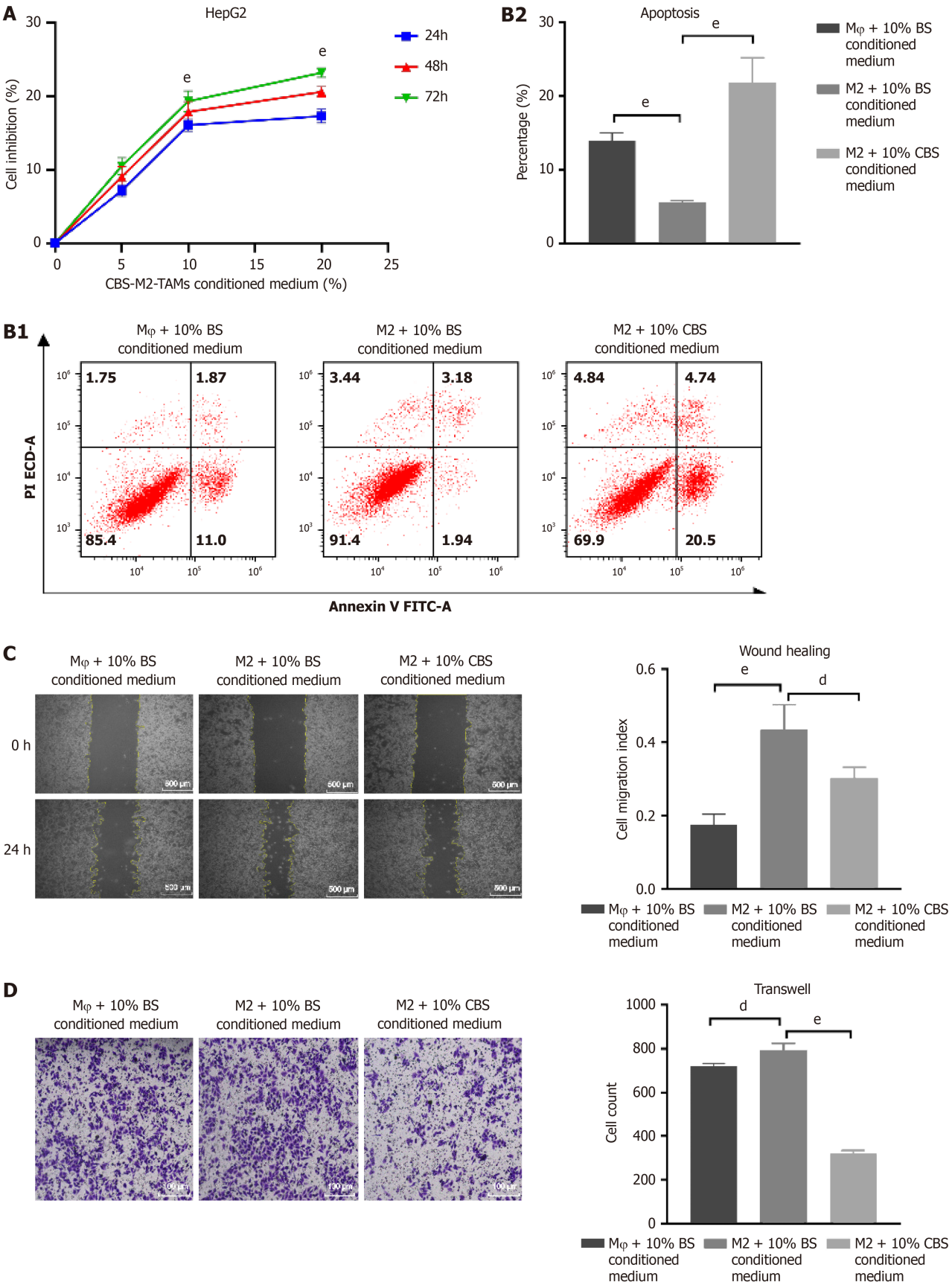

Figure 6 *Calculus bovis*-enriched serum inhibits polarization of M2 tumor-associated macrophages through the Wnt pathway and suppresses malignant behaviors of liver cancer cells. A: Inhibition rate of HepG2 proliferation by M2 + *Calculus bovis*-enriched serum (CBS) conditioned medium; B: Effect of M2 + CBS conditioned medium on HepG2 apoptosis detected by flow cytometry; C: Inhibitory effect of M2 + CBS conditioned medium on migration of HepG2 cells by cell scratch assay; D: Inhibitory effect of M2 + CBS conditioned medium on migration of HepG2 cells by Transwell assay. M2 + CBS conditioned medium: Supernatants of differentiated M2 macrophages cultured in DMEM medium enriched with CBS and penicillin-streptomycin, and the conditional media were

collected after culture. $^{d}P < 0.05$, $^{e}P < 0.01$.

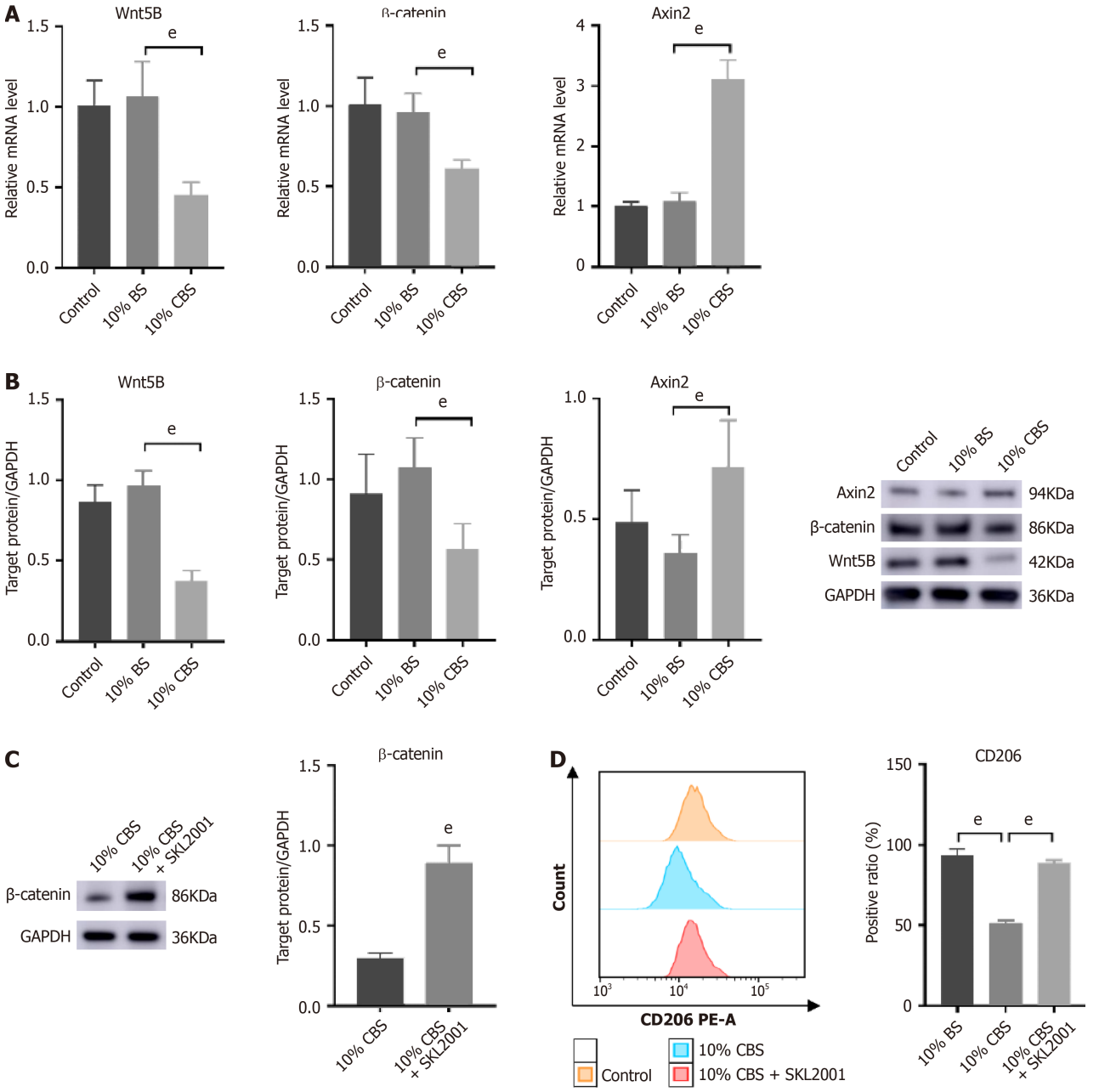

Figure 7 *Calculus bovis*-enriched serum inhibits polarization of M2 tumor-associated macrophages through the Wnt pathway to suppress against liver cancer. A: Effect of *Calculus bovis*-enriched serum (CBS) on *Wnt5B*, *β-catenin*, and *Axin2* mRNA levels in THP-1 cells detected by real-time reverse transcriptase-polymerase chain reaction; B: Effect of CBS on Wnt5B, β-catenin, and Axin2 protein levels in THP-1 cells detected by Western blot analysis; C: Effect of the Wnt pathway agonist SKL2001 on β-catenin protein expression; D: Changes in CD206 detected by flow cytometry in THP-1 cells after CBS combined with SKL2001 intervention for polarization. $^{e}P < 0.01$.

Research has shown that the Wnt pathway is essential to drive liver cancer progression, particularly by upregulating CCL22 and TGF-β2, which are associated with M2 macrophage polarization[44-46]. It has been demonstrated that CB-enriched serum can inhibit M2-TAM polarization stimulated by IL-13/IL-4, reversing the switch to an M2 phenotype and reducing the invasive and migratory capabilities in liver cancer both *in vitro* and *in vivo*. Meanwhile, the presence of SKL2001 indicates that the inhibitory effects of CB on M2-TAM activation can be modulated by the Wnt/β-catenin pathway. The weak direct killing effect on tumor cells exhibited by CB *in vitro* does not completely explain its anti-tumor effects *in vivo*. Therefore, we speculate that immunomodulation may be an important pathway for the anti-tumor activity of CB. This study is the first to demonstrate that CB inhibits liver cancer development by regulating TAM polarization, thereby enhancing our understanding of the pharmacological role of CB and offering a promising and effective treatment option for liver cancer. However, T-cell infiltration, NK cell activation, and PD-1/PD-L1 expression are factors that affect

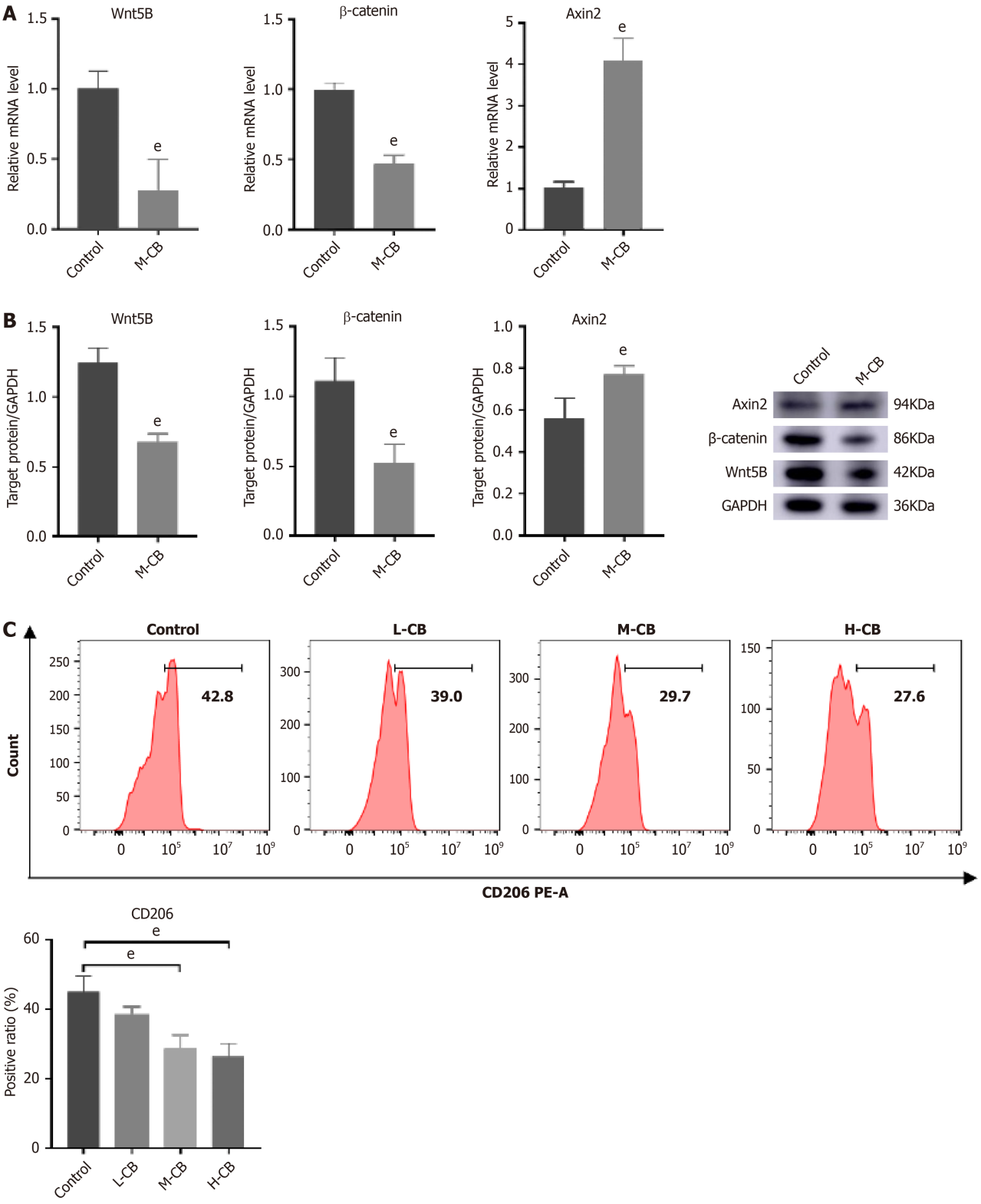

Figure 8 *In vivo* experimental validation of regulation of M2 macrophage polarization by *Calculus bovis* through the Wnt pathway. A: Quantification of mRNA expression of *Wnt5B*, β-catenin, and *Axin2* by real-time reverse transcriptase-polymerase chain reaction; B: Quantification of protein expression of Wnt5B, β-catenin, and Axin2 by Western blot analysis; C: Ratio of cells expressing CD206 molecules in tumor tissues analyzed by flow cytometry. $^{e}P < 0.01$.

the TME, and it is not clear whether CB has a regulatory effect on them, which needs to be addressed in future studies.

We found that there are as many as 22 constituents of CB. However, it is not clear which compounds play a role in regulating macrophage polarization, and this needs to be clarified in future studies. Furthermore, the synergistic effects of these active components with clinical antitumor drugs should be investigated. In addition, new drug development strategies such as structural modifications and targeting system construction should be utilized to enhance the antitumor effects of the active ingredients of CB and improve their targeting properties, making them potential antitumor drugs.

CONCLUSION

CB has long been used in traditional Chinese herbal medicine for its anti-inflammatory and immunomodulatory properties to treat various tumors. The influential anti-inflammatory and immunomodulatory properties of CB make it a potential therapeutic agent against liver cancer by modulating the TME and inhibiting M2-TAM macrophage polarization through the Wnt/β-catenin pathway (Figure 9). Its suppressive effects and ability to target the Wnt pathway offer a novel approach to cancer therapy, potentially leading to progressive advances in malignancy treatment.

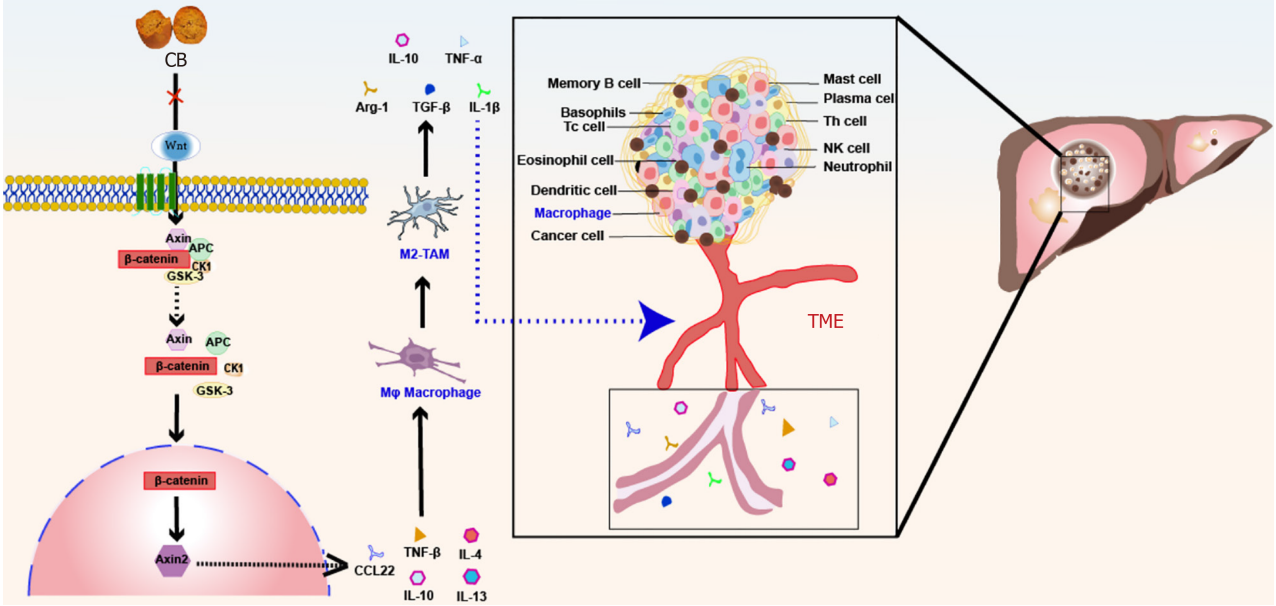

Figure 9 Schematic diagram of anti-liver cancer mechanism of *Calculus bovis*. *Calculus bovis* exerts its anti-liver cancer effect by inhibiting the Wnt/β-catenin pathway and suppressing the polarization of M2 tumor-associated macrophage. M2-TAMs: M2 tumor-associated macrophages; TME: Tumor microenvironment.

FOOTNOTES

Author contributions: Huang Z, Meng FY, Mei S, and Tian XF designed the study; Huang Z, Meng FY, Lu LZ, Guo QQ, Deng Z, Zou B, and Long HP performed the experiments, and acquired and analyzed the data; Huang Z, Meng FY, Lu LZ, and Guo QQ prepared the figures and tables; Huang Z, Meng FY, Lu LZ, Guo QQ, Lv CJ, Tan NH, Deng Z, Chen JY, Zhang ZS, Zhou Q, Mei S, and Tian XF reviewed and edited the manuscript. All authors reviewed and approved the final version of the article. Huang Z and Meng FY are designated as co-first authors due to their nearly equal contributions across various aspects of the project, including study design, data collection and analysis, and manuscript writing. Their dedication and efforts in these crucial stages highlight their high level of collaboration and professional competence, which has ensured the smooth progress and high quality of the research. The comparable workload and impact of both authors justify their co-first author designation, reflecting their significant contributions fairly. Additionally, the research team comprises members with diverse expertise and skills across multiple disciplines. This diversity forms a solid foundation for the study, ensuring its comprehensiveness and reliability. The designation of co-first authors not only exemplifies the collaborative spirit and professional standards within the team but also enhances the scientific rigor and integrity of the paper. The reasons for designating Tian XF and Mei S as co-corresponding authors are threefold. First, both authors have made equally important contributions to the research work and have invested equal amounts of effort in writing the paper and designing the experiments. To be fair, they are listed as co-corresponding authors. Second, both authors have made significant contributions in their respective fields and have assumed different responsibilities in the paper. Their joint communication better reflects the nature of interdisciplinary cooperation. Third, having two corresponding authors provides a wider range of contact channels for readers to communicate and discuss with the research team, improving the dissemination and influence of the research work.

Supported by National Natural Science Foundation of China, No. 82074450; Education Department of Hunan Province, No. 21A0243, No. 21B0374, No. 22B0397, and No. 22B0392; Research Project of "Academician Liu Liang Workstation" of Hunan University of Traditional Chinese Medicine, No. 21YS003; Hunan Administration of Traditional Chinese Medicine, No. B2023001 and No. B2023009; and Hunan Provincial Natural Science Foundation of China, No. 2023JJ40481.

Institutional animal care and use committee statement: All animal experiments were conducted according to a protocol approved by the Ethical Review Committee of Experimental Animal Welfare at Slacker Jingda Laboratory, Changsha, Hunan (No. IACUC-SJA2022105).

Conflict-of-interest statement: The authors declare that they have no competing interests to disclose.

Data sharing statement: Dataset is available from the corresponding author at 003640@hnucm.edu.cn. Participants gave informed consent for data sharing.

ARRIVE guidelines statement: The authors have read the ARRIVE guidelines, and the manuscript was prepared and revised according to the ARRIVE guidelines.

Open-Access: This article is an open-access article that was selected by an in-house editor and fully peer-reviewed by external reviewers. It is distributed in accordance with the Creative Commons Attribution NonCommercial (CC BY-NC 4.0) license, which permits others to distribute, remix, adapt, build upon this work non-commercially, and license their derivative works on different terms, provided the original work is properly cited and the use is non-commercial. See: Https://creativecommons.org/Licenses/by-nc/4.0/

Country of origin: China

ORCID number: Zhen Huang 0000-0002-8437-7141; Zhe Deng 0000-0002-3283-6289; Hong-Ping Long 0000-0001-8891-5851; Qing Zhou 0000-0002-9633-7542; Sha Tian 0000-0002-2557-5674; Si Mei 0000-0002-4263-1121; Xue-Fei Tian 0000-0003-4786-0844.

S-Editor: Qu XL
L-Editor: Wang TQ
P-Editor: Zhao YQ

REFERENCES

1 **Peng J**, Lü M, Peng Y, Tang X. Global incidence of primary liver cancer by etiology among children, adolescents, and young adults. *J Hepatol* 2023; **79**: e92-e94 [PMID: 36841544 DOI: 10.1016/j.jhep.2023.02.019]
2 **Laface C**, Fedele P, Maselli FM, Ambrogio F, Foti C, Molinari P, Ammendola M, Lioce M, Ranieri G. Targeted Therapy for Hepatocellular Carcinoma: Old and New Opportunities. *Cancers (Basel)* 2022; **14** [PMID: 36011021 DOI: 10.3390/cancers14164028]
3 **Muñoz-Martínez S**, Iserte G, Sanduzzi-Zamparelli M, Llarch N, Reig M. Current pharmacological treatment of hepatocellular carcinoma. *Curr Opin Pharmacol* 2021; **60**: 141-148 [PMID: 34418875 DOI: 10.1016/j.coph.2021.07.009]
4 **Rizzo A**, Ricci AD, Brandi G. Trans-Arterial Chemoembolization Plus Systemic Treatments for Hepatocellular Carcinoma: An Update. *J Pers Med* 2022; **12** [PMID: 36579504 DOI: 10.3390/jpm12111788]
5 **Xu B**, Sun HC. Camrelizumab: an investigational agent for hepatocellular carcinoma. *Expert Opin Investig Drugs* 2022; **31**: 337-346 [PMID: 34937475 DOI: 10.1080/13543784.2022.2022121]
6 **Maki H**, Hasegawa K. Advances in the surgical treatment of liver cancer. *Biosci Trends* 2022; **16**: 178-188 [PMID: 35732434 DOI: 10.5582/bst.2022.01245]
7 **Dall'Olio FG**, Rizzo A, Mollica V, Massucci M, Maggio I, Massari F. Immortal time bias in the association between toxicity and response for immune checkpoint inhibitors: a meta-analysis. *Immunotherapy* 2021; **13**: 257-270 [PMID: 33225800 DOI: 10.2217/imt-2020-0179]
8 **Rizzo A**, Mollica V, Tateo V, Tassinari E, Marchetti A, Rosellini M, De Luca R, Santoni M, Massari F. Hypertransaminasemia in cancer patients receiving immunotherapy and immune-based combinations: the MOUSEION-05 study. *Cancer Immunol Immunother* 2023; **72**: 1381-1394 [PMID: 36695827 DOI: 10.1007/s00262-023-03366-x]
9 **Guven DC**, Sahin TK, Erul E, Rizzo A, Ricci AD, Aksoy S, Yalcin S. The association between albumin levels and survival in patients treated with immune checkpoint inhibitors: A systematic review and meta-analysis. *Front Mol Biosci* 2022; **9**: 1039121 [PMID: 36533070 DOI: 10.3389/fmolb.2022.1039121]
10 **Wang K**, Chen Q, Shao Y, Yin S, Liu C, Liu Y, Wang R, Wang T, Qiu Y, Yu H. Anticancer activities of TCM and their active components against tumor metastasis. *Biomed Pharmacother* 2021; **133**: 111044 [PMID: 33378952 DOI: 10.1016/j.biopha.2020.111044]
11 **Rizzo A**, Ricci AD, Brandi G. Immune-based combinations for advanced hepatocellular carcinoma: shaping the direction of first-line therapy. *Future Oncol* 2021; **17**: 755-757 [PMID: 33508960 DOI: 10.2217/fon-2020-0986]
12 **Rizzo A**, Ricci AD, Brandi G. Systemic adjuvant treatment in hepatocellular carcinoma: tempted to do something rather than nothing. *Future Oncol* 2020; **16**: 2587-2589 [PMID: 32772560 DOI: 10.2217/fon-2020-0669]
13 **Rui R**, Zhou L, He S. Cancer immunotherapies: advances and bottlenecks. *Front Immunol* 2023; **14**: 1212476 [PMID: 37691932 DOI: 10.3389/fimmu.2023.1212476]
14 **Li JJ**, Liang Q, Sun GC. Traditional Chinese medicine for prevention and treatment of hepatocellular carcinoma: A focus on epithelial-mesenchymal transition. *J Integr Med* 2021; **19**: 469-477 [PMID: 34538644 DOI: 10.1016/j.joim.2021.08.004]
15 **Shi J**, Zhu L, Tang BY, Yang WQ, Xi SY, Zhang CL, Li PF, Wang YJ, Guo KH, Huang JR, Huang CR, Yu ZX, Yu BK, Zhang CF, Zhang YM. Regulatory effect of Yinchenhao decoction on bile acid metabolism to improve the inflammatory microenvironment of hepatocellular carcinoma in mice. *J Nat Med* 2024; **78**: 633-643 [PMID: 38704807 DOI: 10.1007/s11418-024-01812-3]
16 **Sharma A**, Seow JJW, Dutertre CA, Pai R, Blériot C, Mishra A, Wong RMM, Singh GSN, Sudhagar S, Khalilnezhad S, Erdal S, Teo HM, Khalilnezhad A, Chakarov S, Lim TKH, Fui ACY, Chieh AKW, Chung CP, Bonney GK, Goh BK, Chan JKY, Chow PKH, Ginhoux F, DasGupta R. Onco-fetal Reprogramming of Endothelial Cells Drives Immunosuppressive Macrophages in Hepatocellular Carcinoma. *Cell* 2020; **183**: 377-394.e21 [PMID: 32976798 DOI: 10.1016/j.cell.2020.08.040]
17 **Yunna C**, Mengru H, Lei W, Weidong C. Macrophage M1/M2 polarization. *Eur J Pharmacol* 2020; **877**: 173090 [PMID: 32234529 DOI: 10.1016/j.ejphar.2020.173090]
18 **Sica A**, Erreni M, Allavena P, Porta C. Macrophage polarization in pathology. *Cell Mol Life Sci* 2015; **72**: 4111-4126 [PMID: 26210152 DOI: 10.1007/s00018-015-1995-y]
19 **Yang Y**, Ye YC, Chen Y, Zhao JL, Gao CC, Han H, Liu WC, Qin HY. Crosstalk between hepatic tumor cells and macrophages *via* Wnt/β-catenin signaling promotes M2-like macrophage polarization and reinforces tumor malignant behaviors. *Cell Death Dis* 2018; **9**: 793 [PMID: 30022048 DOI: 10.1038/s41419-018-0818-0]
20 **Mano Y**, Aishima S, Fujita N, Tanaka Y, Kubo Y, Motomura T, Taketomi A, Shirabe K, Maehara Y, Oda Y. Tumor-associated macrophage promotes tumor progression *via* STAT3 signaling in hepatocellular carcinoma. *Pathobiology* 2013; **80**: 146-154 [PMID: 23364389 DOI: 10.1159/000346196]

21 **Cox N**, Pokrovskii M, Vicario R, Geissmann F. Origins, Biology, and Diseases of Tissue Macrophages. *Annu Rev Immunol* 2021; **39**: 313-344 [PMID: 33902313 DOI: 10.1146/annurev-immunol-093019-111748]

22 **Cronan MR**, Beerman RW, Rosenberg AF, Saelens JW, Johnson MG, Oehlers SH, Sisk DM, Jurcic Smith KL, Medvitz NA, Miller SE, Trinh LA, Fraser SE, Madden JF, Turner J, Stout JE, Lee S, Tobin DM. Macrophage Epithelial Reprogramming Underlies Mycobacterial Granuloma Formation and Promotes Infection. *Immunity* 2016; **45**: 861-876 [PMID: 27760340 DOI: 10.1016/j.immuni.2016.09.014]

23 **Fidler IJ**, Schroit AJ. Recognition and destruction of neoplastic cells by activated macrophages: discrimination of altered self. *Biochim Biophys Acta* 1988; **948**: 151-173 [PMID: 3052591 DOI: 10.1016/0304-419x(88)90009-1]

24 **Naramore S**, Virojanapa A, Bell M, Jhaveri PN. Bezoar in a Pediatric Oncology Patient Treated with Coca-Cola. *Case Rep Gastroenterol* 2015; **9**: 227-232 [PMID: 26269699 DOI: 10.1159/000431217]

25 **Dimin N**, Zhe D, Yongrong W, Si M, Yongjie T, Qing Z, Xuefei T. Niuhuang (Bovis Calculus)-Shexiang (Moschus) combination induces apoptosis and inhibits proliferation in hepatocellular carcinoma *via* PI3K/AKT/mTOR pathway. *Digit Chin Med* 2022; **5**: 83-92 [DOI: 10.1016/j.dcmed.2022.03.009]

26 **Yu ZJ**, Xu Y, Peng W, Liu YJ, Zhang JM, Li JS, Sun T, Wang P. Calculus bovis: A review of the traditional usages, origin, chemistry, pharmacological activities and toxicology. *J Ethnopharmacol* 2020; **254**: 112649 [PMID: 32068140 DOI: 10.1016/j.jep.2020.112649]

27 **Zhang Z**, Zeng P, Gao W, Wu R, Deng T, Chen S, Tian X. Exploration of the Potential Mechanism of Calculus Bovis in Treatment of Primary Liver Cancer by Network Pharmacology. *Comb Chem High Throughput Screen* 2021; **24**: 129-138 [PMID: 32772910 DOI: 10.2174/1386207323666200808172051]

28 **Xiang D**, Liu Y, Zu Y, Yang J, He W, Zhang C, Liu D. Calculus Bovis Sativus alleviates estrogen cholestasis-induced gut and liver injury in rats by regulating inflammation, oxidative stress, apoptosis, and bile acid profiles. *J Ethnopharmacol* 2023; **302**: 115854 [PMID: 36273746 DOI: 10.1016/j.jep.2022.115854]

29 **Deng Y**, Ren H, Ye X, Xia L, Liu M, Liu Y, Yang M, Yang S, Ye X, Zhang J. Integrated Phytochemical Analysis Based on UPLC-Q-TOF-MS/MS, Network Pharmacology, and Experiment Verification to Explore the Potential Mechanism of Platycodon grandiflorum for Chronic Bronchitis. *Front Pharmacol* 2020; **11**: 564131 [PMID: 33013400 DOI: 10.3389/fphar.2020.564131]

30 **Liu H**, Mohammed SAD, Lu F, Chen P, Wang Y, Liu S. Network Pharmacology and Molecular Docking-Based Mechanism Study to Reveal Antihypertensive Effect of Gedan Jiangya Decoction. *Biomed Res Int* 2022; **2022**: 3353464 [PMID: 36046450 DOI: 10.1155/2022/3353464]

31 **Pai SG**, Carneiro BA, Mota JM, Costa R, Leite CA, Barroso-Sousa R, Kaplan JB, Chae YK, Giles FJ. Wnt/beta-catenin pathway: modulating anticancer immune response. *J Hematol Oncol* 2017; **10**: 101 [PMID: 28476164 DOI: 10.1186/s13045-017-0471-6]

32 **Miao TG**, Nan YM. [Hepatocellular carcinoma immune microenvironment]. *Zhonghua Gan Zang Bing Za Zhi* 2022; **30**: 923-930 [PMID: 36299184 DOI: 10.3760/cma.j.cn501113-20220703-00365]

33 **Gou H**, Su H, Liu D, Wong CC, Shang H, Fang Y, Zeng X, Chen H, Li Y, Huang Z, Fan M, Wei C, Wang X, Zhang X, Li X, Yu J. Traditional Medicine Pien Tze Huang Suppresses Colorectal Tumorigenesis Through Restoring Gut Microbiota and Metabolites. *Gastroenterology* 2023; **165**: 1404-1419 [PMID: 37704113 DOI: 10.1053/j.gastro.2023.08.052]

34 **Xu HB**, Chen XZ, Wang X, Pan J, Yi-Zhuo Z, Zhou CH. Xihuang pill in the treatment of cancer: TCM theories, pharmacological activities, chemical compounds and clinical applications. *J Ethnopharmacol* 2023; **316**: 116699 [PMID: 37257709 DOI: 10.1016/j.jep.2023.116699]

35 **Wang W**, Smits R, Hao H, He C. Wnt/β-Catenin Signaling in Liver Cancers. *Cancers (Basel)* 2019; **11** [PMID: 31269694 DOI: 10.3390/cancers11070926]

36 **Long G**, Wu Z, Wang D, Mi X, Hu K, Zhou L, Tang J. UCHL3 inhibits ferroptosis by stabilizing β-catenin and maintains stem-like properties of hepatocellular carcinoma cells. *Free Radic Biol Med* 2024; **212**: 162-173 [PMID: 38092274 DOI: 10.1016/j.freeradbiomed.2023.11.030]

37 **Chen Y**, Yang Y, Wang N, Liu R, Wu Q, Pei H, Li W. β-Sitosterol suppresses hepatocellular carcinoma growth and metastasis *via* FOXM1-regulated Wnt/β-catenin pathway. *J Cell Mol Med* 2024; **28**: e18072 [PMID: 38063438 DOI: 10.1111/jcmm.18072]

38 **Sen B**, Aggarwal S, Nath R, Sehgal R, Singh R, Agrawal K, Shashidhara AN, Rastogi A, Bajpai M, Pamecha V, Trehanpati N, Ramakrishna G. Secretome of senescent hepatoma cells modulate immune cell fate by macrophage polarization and neutrophil extracellular traps formation. *Med Oncol* 2022; **39**: 134 [PMID: 35726030 DOI: 10.1007/s12032-022-01732-w]

39 **Li XY**, Su L, Jiang YM, Gao WB, Xu CW, Zeng CQ, Song J, Xu Y, Weng WC, Liang WB. The Antitumor Effect of Xihuang Pill on Treg Cells Decreased in Tumor Microenvironment of 4T1 Breast Tumor-Bearing Mice by PI3K/AKT~AP-1 Signaling Pathway. *Evid Based Complement Alternat Med* 2018; **2018**: 6714829 [PMID: 29849718 DOI: 10.1155/2018/6714829]

40 **Xiang X**, Wang J, Lu D, Xu X. Targeting tumor-associated macrophages to synergize tumor immunotherapy. *Signal Transduct Target Ther* 2021; **6**: 75 [PMID: 33619259 DOI: 10.1038/s41392-021-00484-9]

41 **Cutolo M**, Campitiello R, Gotelli E, Soldano S. The Role of M1/M2 Macrophage Polarization in Rheumatoid Arthritis Synovitis. *Front Immunol* 2022; **13**: 867260 [PMID: 35663975 DOI: 10.3389/fimmu.2022.867260]

42 **Li Y**, Jin K, van Pelt GW, van Dam H, Yu X, Mesker WE, Ten Dijke P, Zhou F, Zhang L. c-Myb Enhances Breast Cancer Invasion and Metastasis through the Wnt/β-Catenin/Axin2 Pathway. *Cancer Res* 2016; **76**: 3364-3375 [PMID: 27197202 DOI: 10.1158/0008-5472.CAN-15-2302]

43 **Wu Y**, Zheng L. Dynamic education of macrophages in different areas of human tumors. *Cancer Microenviron* 2012; **5**: 195-201 [PMID: 22696271 DOI: 10.1007/s12307-012-0113-z]

44 **Wang C**, Shen N, Guo Q, Tan X, He S. YAP/STAT3 inhibited CD8(+) T cells activity in the breast cancer immune microenvironment by inducing M2 polarization of tumor-associated macrophages. *Cancer Med* 2023; **12**: 16295-16309 [PMID: 37329188 DOI: 10.1002/cam4.6242]

45 **de Carvalho TG**, Lara P, Jorquera-Cordero C, Aragão CFS, de Santana Oliveira A, Garcia VB, de Paiva Souza SV, Schomann T, Soares LAL, da Matta Guedes PM, de Araújo Júnior RF. Inhibition of murine colorectal cancer metastasis by targeting M2-TAM through STAT3/NF-kB/AKT signaling using macrophage 1-derived extracellular vesicles loaded with oxaliplatin, retinoic acid, and Libidibia ferrea. *Biomed Pharmacother* 2023; **168**: 115663 [PMID: 37832408 DOI: 10.1016/j.biopha.2023.115663]

46 **He S**, Lu M, Zhang L, Wang Z. RSK4 promotes the macrophage recruitment and M2 polarization in esophageal squamous cell carcinoma. *Biochim Biophys Acta Mol Basis Dis* 2024; **1870**: 166996 [PMID: 38142759 DOI: 10.1016/j.bbadis.2023.166996]

Published by **Baishideng Publishing Group Inc**
7041 Koll Center Parkway, Suite 160, Pleasanton, CA 94566, USA
Telephone: +1-925-3991568
E-mail: office@baishideng.com
Help Desk: https://www.f6publishing.com/helpdesk
https://www.wjgnet.com

© 2024 Baishideng Publishing Group Inc. All rights reserved.